iScience

CellPress

Article

Trans-omic Analysis Reveals Selective Responses to Induced and Basal Insulin across Signaling, Transcriptional, and Metabolic Networks

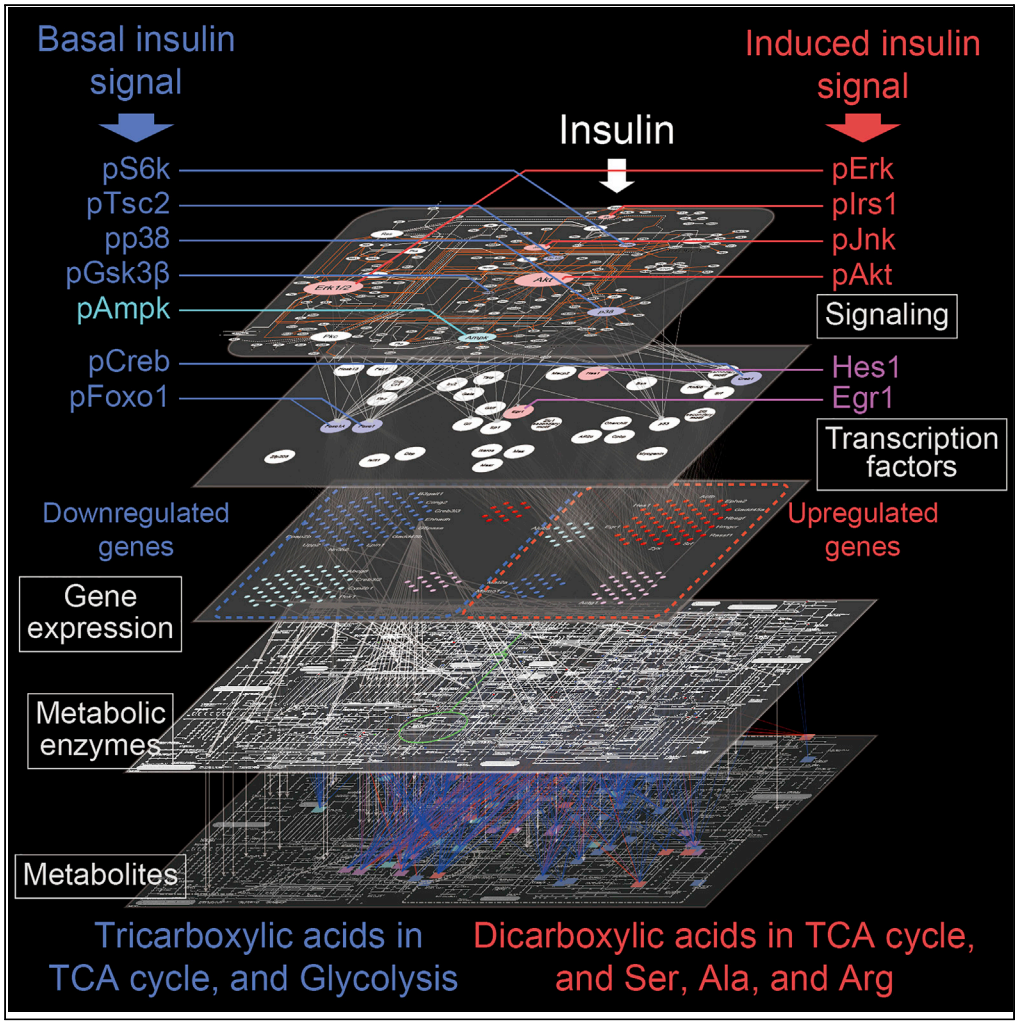

Kentaro Kawata, Atsushi Hatano, Katsuyuki Yugi, ..., Akiyoshi Hirayama, Tomoyoshi Soga, Shinya Kuroda

skuroda@bs.s.u-tokyo.ac.jp

HIGHLIGHTS

We constructed a trans-omic network of insulin action using multi-omic data

The trans-omic network integrates phosphorylation, transcription, and metabolism

We divided induced- and basal-insulin-dependent trans-omic network by sensitivity

Induced and basal insulin triggered selective trans-omic network in the liver

Kawata et al., iScience 7, 212–229
September 28, 2018
https://doi.org/10.1016/j.isci.2018.07.022

iScience

CellPress

Article

Trans-omic Analysis Reveals Selective Responses to Induced and Basal Insulin across Signaling, Transcriptional, and Metabolic Networks

Kentaro Kawata,[1,11,13] Atsushi Hatano,[1,13] Katsuyuki Yugi,[1,2,3,9,13] Hiroyuki Kubota,[6] Takanori Sano,[5,12] Masashi Fujii,[1,4] Yoko Tomizawa,[1] Toshiya Kokaji,[5] Kaori Y. Tanaka,[5] Shinsuke Uda,[6] Yutaka Suzuki,[5] Masaki Matsumoto,[7] Keiichi I. Nakayama,[7] Kaori Saitoh,[8] Keiko Kato,[8] Ayano Ueno,[8] Maki Ohishi,[8] Akiyoshi Hirayama,[8] Tomoyoshi Soga,[8] and Shinya Kuroda[1,5,10,14,*]

SUMMARY

The concentrations of insulin selectively regulate multiple cellular functions. To understand how insulin concentrations are interpreted by cells, we constructed a trans-omic network of insulin action in FAO hepatoma cells using transcriptomic data, western blotting analysis of signaling proteins, and metabolomic data. By integrating sensitivity into the trans-omic network, we identified the selective trans-omic networks stimulated by high and low doses of insulin, denoted as induced and basal insulin signals, respectively. The induced insulin signal was selectively transmitted through the pathway involving Erk to an increase in the expression of immediate-early and upregulated genes, whereas the basal insulin signal was selectively transmitted through a pathway involving Akt and an increase of Foxo phosphorylation and a reduction of downregulated gene expression. We validated the selective trans-omic network *in vivo* by analysis of the insulin-clamped rat liver. This integrated analysis enabled molecular insight into how liver cells interpret physiological insulin signals to regulate cellular functions.

INTRODUCTION

Metabolic disorders involving insulin resistance are a major health concern (Zimmet et al., 2001). Insulin controls organismal metabolic homeostasis by regulating multiple cellular functions, including gene expression, metabolism, and protein synthesis in target organs, such as the liver, skeletal muscle, and adipose tissue (Jastrzebski et al., 2007; Saltiel and Kahn, 2001; Whiteman et al., 2002). Understanding how cells interpret this physiologically dynamic hormone may provide new insights into preventing or treating metabolic disorders associated with insulin resistance. In the liver, insulin activates signaling proteins, such as the kinases Akt, and extracellular-signal-regulated kinase (Erk) (Lizcano and Alessi, 2002; Saltiel and Kahn, 2001); regulates protein abundance through transcriptional or translational mechanisms (Titchenell et al., 2017); and controls cellular metabolite composition, including glycolysis, gluconeogenesis, glycogenesis, amino acid metabolism, and lipid metabolism, by regulating the abundance and activity of metabolic enzymes (Saltiel and Kahn, 2001; Titchenell et al., 2017).

As with many hormones, the release of insulin varies and the cellular response is also complex and changes over time (Brabant et al., 1992; Lindsay et al., 2003; O'Meara et al., 1993; O'Rahilly et al., 1988; Polonsky et al., 1988). Glucose induces the secretion of insulin from the pancreas, resulting in a transient high concentration of insulin in the blood (induced insulin secretion) during the fed state, whereas under basal conditions, a sustained low concentration of insulin (basal insulin secretion) is maintained in the blood during the fasting state (Lindsay et al., 2003; Polonsky et al., 1988). Abnormalities in temporal patterns of insulin secretion and the consequent abnormal concentrations of circulating insulin contribute to the pathogenesis of type 2 diabetes mellitus, indicating that the metabolic response to insulin depends on its temporal patterns (Polonsky et al., 1988). To respond properly to insulin, cells must detect both induced and basal insulin signals and properly interpret each type of insulin signal. We previously showed that signaling proteins, such as Akt (Kubota et al., 2012, 2018); metabolites, such as glycogen (Noguchi et al., 2013); and genes, such as *glucose-6-phosphatase* (*G6Pase*) and *phosphoenolpyruvate carboxykinase1* (*Pck1*) (Sano

[1]Department of Biological Sciences, Graduate School of Science, University of Tokyo, 7-3-1 Hongo, Bunkyo-ku, Tokyo 113-0033, Japan

[2]YCI Laboratory for Trans-Omics, Young Chief Investigator Program, RIKEN Center for Integrative Medical Science, 1-7-22 Suehiro-cho, Tsurumi-ku, Yokohama, Kanagawa 230-0045, Japan

[3]Institute for Advanced Biosciences, Keio University, Fujisawa 252-8520, Japan

[4]Molecular Genetics Research Laboratory, Graduate School of Science, University of Tokyo, 7-3-1 Hongo, Bunkyo-ku, Tokyo 113-0033, Japan

[5]Department of Computational Biology and Medical Sciences, Graduate School of Frontier Sciences, University of Tokyo, 5-1-5 Kashiwanoha, Kashiwa, Chiba 277-8562, Japan

[6]Division of Integrated Omics, Research Center for Transomics Medicine, Medical Institute of Bioregulation, Kyushu University, 3-1-1 Maidashi, Higashi-ku, Fukuoka 812-8582, Japan

[7]Department of Molecular and Cellular Biology, Medical Institute of Bioregulation, Kyushu University, 3-1-1 Maidashi, Higashi-ku, Fukuoka 812-8582, Japan

[8]Institute for Advanced Biosciences, Keio University, 246-2 Mizukami, Kakuganji, Tsuruoka, Yamagata 997-0052, Japan

Continued

et al., 2016), show distinct changes in the activity, abundance, or expression in response to a transient high dose or a sustained low dose of insulin. However, the pathways that selectively transmit the induced and basal insulin signals to regulate selective functions have yet to be analyzed.

Various omic studies of insulin action have used phosphoproteome (Friedman et al., 2011; Humphrey et al., 2013, 2015; Krüger et al., 2008; Monetti et al., 2011; Vinayagam et al., 2016; Yugi et al., 2014; Zhang et al., 2017), transcriptome (Dupont et al., 2001; Hectors et al., 2012; Kim and Lee, 2014; Rome et al., 2003; Sano et al., 2016; Versteyhe et al., 2013), or metabolome data (Everman et al., 2016; Noguchi et al., 2013; Yugi et al., 2014). Individually, each of these can be studied with existing technologies, but the challenge is integrating disparate types of omic data to generate a more comprehensive view of the cellular response than can be gained from one type of data alone (Yugi and Kuroda, 2017; Yugi et al., 2016). We propose "trans-omics" as a discipline for constructing molecular interaction networks across multiple omic datasets using inferred or measured direct molecular interactions rather than indirect statistical relationships (Yugi and Kuroda, 2017; Yugi et al., 2014, 2016). Trans-omic analyses of networks controlling metabolism have been reported for *Escherichia coli* (Gerosa et al., 2015; Ishii et al., 2007), *Bacillus subtilis* (Buescher et al., 2012), *Saccharomyces cerevisiae* (Gonçalves et al., 2017; Hackett et al., 2016; Oliveira et al., 2012), Chinese hamster ovary cells (Yusufi et al., 2017), and human T cells (Geiger et al., 2016). We have previously constructed trans-omic networks of the regulation of metabolism through phosphorylation in response to acute insulin action, in which cells were stimulated with 1 nM insulin for 60 min, with phosphoproteomic and metabolomic data (Yugi et al., 2014). However, how induced and basal insulin signals selectively regulate the trans-omic network is yet to be analyzed.

Here, we explored how the hepatoma cell line FAO cells interpret a physiologically dynamic stimulus, induced and basal insulin stimulation. We extended the method for performing trans-omics analysis and constructed a multi-omic network connecting the transcriptome to signaling proteins and transcription factors (TFs) and connecting the transcriptome to the metabolome to explore the role of gene regulation in the metabolic response to insulin. We measured the time course of transcriptomic changes, changes in the activity of signaling proteins by western blotting, and metabolomic changes with different doses of insulin. We used the sensitivity and time constant of the response to insulin to classify insulin-responsive genes (IRGs), signaling molecules, and insulin-responsive metabolites (IRMs) into those that selectively responded to induced or basal insulin stimulation. With the trans-omic network constructed from the multi-omic data, we identified the selective trans-omic network that mediated transcriptional responses to induced and basal insulin stimulation. We validated the physiological relevance of the selective trans-omic networks in the insulin-clamped rat liver. Our study identified mechanisms by which insulin dynamics programs cellular metabolism through transcriptional regulation and regulation of protein translation. This integration of sensitivity and response time data into a trans-omic network can be applied to other complex dynamic regulatory systems to understand the principles by which cells interpret dynamic stimuli.

RESULTS

Procedures for the Trans-omic Network Construction by Induced and Basal Insulin Stimulation

During the postprandial state, insulin secretion is induced producing a transiently high concentration (approximately in the nanomolar range) in the blood (induced insulin); in the fasting state, insulin secretion is low, resulting in a low concentration (approximately in the tens to hundreds of picomolar range) of insulin in the blood (basal insulin) (Lindsay et al., 2003; Polonsky et al., 1988), meaning that sub-nanomolar level of insulin is the threshold between induced and basal insulin secretion (Figure 1A). Induced and basal insulin stimulation selectively regulate physiological functions, such as metabolism (Polonsky et al., 1988). How induced and basal insulin signals are selectively decoded by cells remain unknown. We constructed a trans-omic network to discover the selective pathways of transcriptional regulation and regulation of protein translation that mediate the changes in cellular metabolism by induced and basal insulin stimulation (Scheme S1). We quantified the amounts or the activities of cellular components of rat FAO hepatoma cells stimulated with various doses of insulin and time points—RNA (transcriptomic analysis), key signaling proteins and TFs (western blotting), and metabolites (metabolomic analysis). We classified the transcripts, proteins, and metabolites according to sensitivity to insulin concentration and the time constant of their change in response to 100 nM insulin. With the multi-omic datasets, we constructed the trans-omic network in 3 steps (Figure 1B, Steps I–III). In Step I,

[9]PRESTO, Japan Science and Technology Agency, 1-7-22 Suehiro-cho, Tsurumi-ku, Yokohama, Kanagawa 230-0045, Japan

[10]Core Research for Evolutional Science and Technology (CREST), Japan Science and Technology Agency, Bunkyo-ku, Tokyo 113-0033, Japan

[11]Present address: Isotope Science Center, University of Tokyo, 2-11-16 Yayoi, Bunkyo-ku, Tokyo 113-0032, Japan

[12]Present address: Department of Anatomy and Cell Biology, Graduate School of Medical Sciences, Kyushu University, 3-1-1 Maidashi, Higashi-ku, Fukuoka 812-8582, Japan

[13]These authors contributed equally

[14]Lead Contact

*Correspondence: skuroda@bs.s.u-tokyo.ac.jp

https://doi.org/10.1016/j.isci.2018.07.022

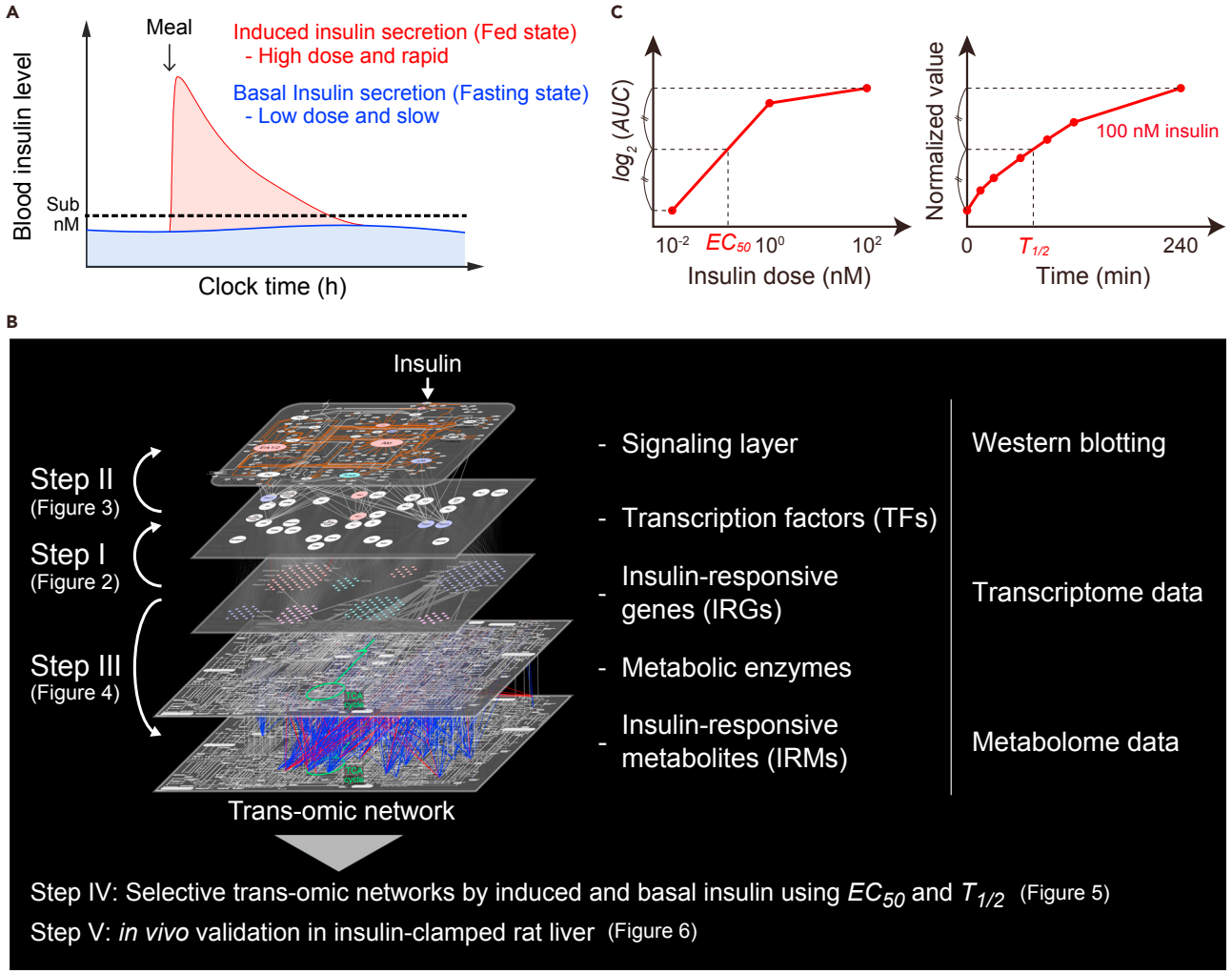

Figure 1. Summary of Procedures for Trans-omic Network Construction

(A) Induced and basal insulin secretion *in vivo* (Polonsky et al., 1988).

(B) The trans-omic network was constructed through Steps I to III by integrating transcriptome, protein (western blotting), and metabolome data. The detailed procedures can be found in Methods.

(C) Definition of EC_{50}, an index of sensitivity to insulin doses (left), and $T_{1/2}$, an index of time constant (right).

we integrated the IRGs identified by transcriptomic analysis and the TFs predicted to regulate the IRGs. In Step II, we integrated the TFs and the signaling layer. In Step III, we integrated the IRMs identified by metabolomic analysis and the IRGs that encode proteins involved in the synthesis and catabolism of the IRMs.

In Step IV, we integrated the result of Steps I–III and constructed a trans-omic network of insulin action with connections within (intra-omic) and between (inter-omic) the layers that mediate signaling responses, transcriptional responses, and changes in cellular metabolism. To map induced and basal insulin-stimulated pathways through the trans-omic network, we estimated the sensitivity (EC_{50}) and time constant ($T_{1/2}$) of the changes in IRG expression, signaling protein activity, and IRM abundance to different concentrations of insulin and periods of exposure to insulin (Figure 1C). Using the sensitivity (EC_{50}) and response time ($T_{1/2}$) data, we identified how induced or basal insulin stimulation resulted in selective inter- and intra-omic pathways through the trans-omic network. In Step V, we tested the accuracy of the FAO cell responses to insulin by comparing a subset of the responses to those obtained with the insulin-clamped rat liver and showed how the data could be integrated with the trans-omic network to understand how signaling through the trans-network resulted in the observed outcomes.

Step I: Connection of the IRGs and the TFs

Step I-I: Selective Gene Expression of Cellular Functions by Induced and Basal Insulin Stimulation

We previously measured the transcriptome in insulin-stimulated FAO cells and analyzed only 13 upregulated and 16 downregulated genes in detail (Sano et al., 2016). Here, we used the complete transcriptomic dataset consisting of 3 doses of insulin (0.01, 1, 100 nM) at 7 time points up to 4 hr. First, we defined 433 genes as IRGs. Using criteria that identify IRGs with smaller variation and larger responses, we categorized the IRGs as 114 upregulated, 144 downregulated, and 175 other IRGs that exhibited variable responses (Figures S1A–S1C, see Methods). The downregulated IRGs included *G6pase* and *Pck1* (Table S1), known to be downregulated in response to insulin (Sano et al., 2016). We estimated the sensitivity from the EC_{50} of the IRGs, which we defined as the dose of insulin that produced 50% of the maximal area under the curve (*AUC*) of a time series of gene expression (Figure 1C, see Methods). The distribution of the EC_{50} values of the IRGs was bimodal (Figure 2A) with the threshold between the modes being an EC_{50} value of 0.70 nM, between the concentrations of induced and basal insulin (Figure 1A), suggesting that induced and basal insulin stimulation selectively control the expression of different gene sets. Furthermore, most of the upregulated IRGs had EC_{50} values higher than 0.70 nM and most of the downregulated IRGs had values lower than 0.70 nM (Figure 2A; Table 1), indicating that the majority of the upregulated IRGs respond to induced insulin stimulation, whereas the majority of the downregulated IRGs respond to basal insulin stimulation. This finding is consistent with our previous study (Sano et al., 2016).

To delineate the functional roles of the up- and downregulated IRGs, we performed Gene Ontology (GO) analysis and Kyoto Encyclopedia of Genes and Genomes (KEGG) pathway enrichment analysis against the gene sets classified by EC_{50} values. The upregulated IRGs showing high sensitivity to insulin were enriched for genes associated with the cytoskeleton, whereas the downregulated IRGs showing low sensitivity to insulin were enriched for genes involved in metabolism (Table S2), indicating that the up- and downregulated IRGs control different cellular functions.

We estimated the response time from the $T_{1/2}$, which we defined as the time when the change in gene expression reached 50% of the peak amplitude (Figure 1C, see Methods). The distribution of the $T_{1/2}$ values of the IRGs was also bimodal (Figure 2A). Unlike EC_{50} values, the $T_{1/2}$ values of the up- and downregulated IRGs showed similar distributions (Figure 2A). The threshold of the bimodal distribution of the $T_{1/2}$ values was 88 min (Table 1). With these calculations, we categorized the IRGs into those with a fast response to induced insulin stimulation ($<T_{1/2}$ of 88 min) and those with a slow response ($>T_{1/2}$ of 88 min). GO analysis of the upregulated IRGs revealed that the upregulated IRGs with a fast response include TFs, such as the immediate-early genes (IEGs), *Egr1*, *Hes1*, and *Srf*. Those showing a slow response include genes related to GO terms such as "actin-filament binding" and "enzyme binding." Finding TFs as fast responding IRGs indicated the stimulation of a successive transcriptional cascade such that induced insulin stimulation initially upregulates the IEGs and the expressed IEG products subsequently induce genes of various cellular functions. Many downregulated IRGs relate to metabolism. Taken together, these results indicated that induced and basal insulin stimulation of FAO cells elicit selective expression of genes with distinct cellular functions.

Step I-II: Prediction of the TFs that Regulate the IRGs according to Sensitivity and Time Constants

Within the up- or downregulated IRGs, we identified 4 classes using the EC_{50} threshold to set high and low insulin sensitivity and the $T_{1/2}$ threshold to set fast and slow response times. The 4 classes are IRGs with high sensitivity (EC_{50} < threshold) and fast response times ($T_{1/2}$ < threshold) (Class 1), high sensitivity and slow response times (Class 2), low sensitivity and fast response times (Class 3), and low sensitivity and slow response times (Class 4) (Figures 2B and S1D; Table S1). These different properties of the IRGs suggested that each class is regulated by different sets of TFs. We identified the over-represented TF binding motifs within the promoters of the IRGs and assigned TFs to each class of the up- and downregulated IRGs (see Methods). Approximately 50% of the upregulated IRGs belong to Class 3 (low sensitivity and fast response) and include the genes encoding TFs such as *Hes1*, *Srf*, and *Egr1*, indicating that expression of these genes increased mainly in response to induced insulin stimulation. More than 80% of the downregulated IRGs belong to Class 1 and 2 (high sensitivity) and include the genes encoding metabolic enzymes, such as *G6pase* (Class 1) and *Pck1* (Class 2) (Table S1). Genes in Classes 1 and 2 are expected to respond to basal insulin stimulation.

Using TRANSFAC, we identified consensus binding motifs for 282 TFs in the 114 upregulated and the 144 downregulated IRGs (Table S3, see Methods). We determined the common TFs predicted to regulate the

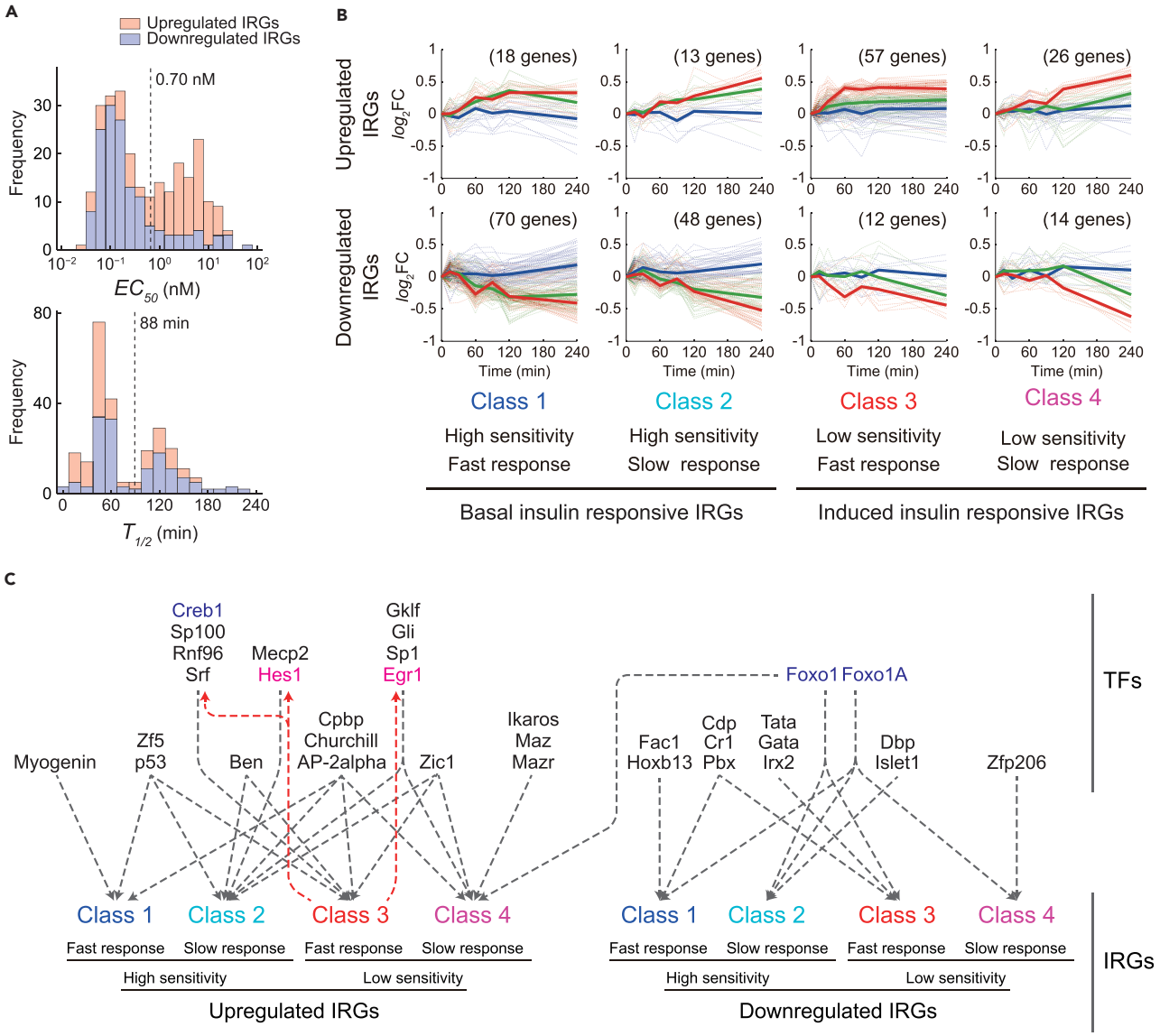

Figure 2. Step I: Connection of the IRGs and the TFs

(A) Distributions of EC_{50} (upper) and $T_{1/2}$ (lower) values estimated for the upregulated IRGs (red bars) and the downregulated IRGs (blue bars). The dashed lines indicate the thresholds of the bimodal distributions.

(B) Time courses of the IRGs in each class classified by the EC_{50} and $T_{1/2}$ values of the IRGs with high or low sensitivity and with fast or slow time constant. Blue, green, and red bold lines represent the averaged responses to 0.01, 1, and 100 nM insulin, respectively. Dashed lines indicate the time series of each IRG in the class. The y axis indicates the base 2 logarithm of fold change against expression of each gene at time 0 (log_2FC).

(C) The TFs predicted for each class of IRGs. Gray dashed arrows indicate the transcriptional regulation by the TFs, and red dashed arrows indicate that the Class 3 IRGs encode the TFs. The color code of the class is the same as in (B). The colored TFs are encoded by TFs of the matching class in Figure 3B: Creb1, Foxo, Foxo1A encoded by Class 1 TF; Hes1 and Egr1 encoded by Class 3 TFs.

See also Figure S1, and Tables S1, S2, and S3.

IRGs in each class. A total of 22 TFs were assigned to the upregulated IRGs and 12 TFs to the downregulated IRGs (Figure 2C; Table S3). We confirmed the TF predictions using data from the ChIP-Seq Atlas (Figure S2). Consistent with reported transcriptional regulation, our analysis identified Foxo1 as a TF for *G6pase* and *Pck1* (Titchenell et al., 2017) and Srf as a TF for the IEGs *Jun* and *Egr1* (Gregg and Fraizer, 2011). Except for Foxo1, the TFs assigned to the up- or downregulated IRGs were mutually exclusive, suggesting that the up- and downregulated IRGs are regulated by different upstream signaling pathways (Figure 2C). The TFs of the upregulated IRGs included Creb, Srf, Hes1, and Egr1, which are downstream of Erk

		Average	Median	p Value	Adjusted p Value	Mode	
						< Threshold	> Threshold
EC_{50} (nM)	Upregulated IRGs	1.6	2.2	9.64×10^{-15}	3.86×10^{-14}	0.25	6.3
	Downregulated IRGs	0.25	0.16			0.10	1.0
	Increased IRMs	4.9	6.6	1.34×10^{-10}	5.36×10^{-10}	0.40	1.6
	Decreased IRMs	1.3	1.2			0.060	0.63
$T_{1/2}$ (min)	Upregulated IRGs	68	50	9.82×10^{-5}	3.93×10^{-4}	45	120
	Downregulated IRGs	86	59			45	120
	Increased IRMs	56	68	1.90×10^{-3}	7.60×10^{-3}	0	105
	Decreased IRMs	18	11			15	60

Table 1. Averages and Medians of EC_{50} and $T_{1/2}$ Values in Insulin-Responsive Genes (IRGs) and Insulin-Responsive Metabolites (IRMs)

(Deak et al., 1998; Murphy et al., 2004; Nakayama et al., 2008; Shaul and Seger, 2007). *Hes1* and *Egr1* were both Class 3 (low sensitivity and fast response) upregulated IRGs, and many of the upregulated Class 3 and Class 4 IRGs had consensus motifs for these 2 TFs, suggesting that Hes1 and Egr1 are key transcriptional regulators of a successive transcriptional cascade activated by the Erk signaling pathway. Downregulated IRGs of each class included those with consensus motifs for TFs of the Foxo family, either Foxo1 or Foxo1A. The transcriptional regulatory activity of Foxo1 and Foxo1A is inhibited by Akt-mediated phosphorylation (Biggs et al., 1999; Brunet et al., 1999), indicating that the inhibition of these proteins is a key mechanism by which the Akt pathway downregulates gene expression.

Given that the majority of the upregulated IRGs responds to induced insulin stimulation, induced insulin stimulation is likely to regulate the upregulated IRGs through Erk signaling pathway followed by the successive transcriptional cascade initiated by the IEGs. Given that the majority of the downregulated IRGs responds to basal insulin stimulation, basal insulin stimulation is likely to regulate the downregulated IRGs through the Akt pathway followed by Foxo proteins' phosphorylation in a posttranscriptional manner. Thus, the analysis indicated that induced and basal insulin stimulation selectively regulate the up- and downregulated IRGs by different mechanisms, induction of a 2-part transcriptional cascade or direct post-translational regulation of a master TF, respectively.

Step II: Connection of the TFs and the Signaling Layer

To integrate the signaling proteins into the trans-omic network, we connected the signaling proteins to the TFs, which were connected to the IRGs. We used the KEGG signaling pathways to connect the TFs to signaling proteins from phosphoproteomic analysis of acute insulin action in our previous study (Yugi et al., 2014). Using the 1,947 insulin-responsive phosphoproteins (Yugi et al., 2014), we constructed a signaling layer by integrating 15 KEGG signaling pathways in which the phosphoproteins were significantly over-represented into the trans-omic network (Figures 3A and S3A; Table S4). Hereafter, we denoted this integrated signaling layer as the signaling layer. On this signaling layer, insulin transmits its signal to 2 major signaling pathways, Akt and Erk pathways through the phosphorylation of Irs via insulin receptor. The signaling layer also includes major kinases; protein synthesis-related factors, which are downstream of Akt-mTOR pathway; and TFs, 10 of which were estimated in Figure 2C (Figure 3A). Several other proteins in the signaling layer connected insulin-responsive signaling events to the TFs that are connected to the IRGs.

We performed sensitivity and response time analysis of a subset of the proteins in the signaling layer and a subset of the TFs predicted to regulate the IRGs. In the signaling layer, we selected proteins involved in the regulation of protein synthesis and proteins involved in the regulation of transcription. We measured the amount or phosphorylation level of these proteins using commercially available antibodies and estimated their EC_{50} and $T_{1/2}$ values (Figures 3B, 3C, S3B, and S3C; Table S5). We divided the signaling proteins into classes by determining thresholds of the EC_{50} and the $T_{1/2}$ values using Otsu's method (Otsu, 1979). We classified the signaling proteins, as we did the IRGs, into 4 classes (Figure 3C). The threshold for signaling proteins was 0.63 nM, which is similar to that of IRGs (0.70 nM).

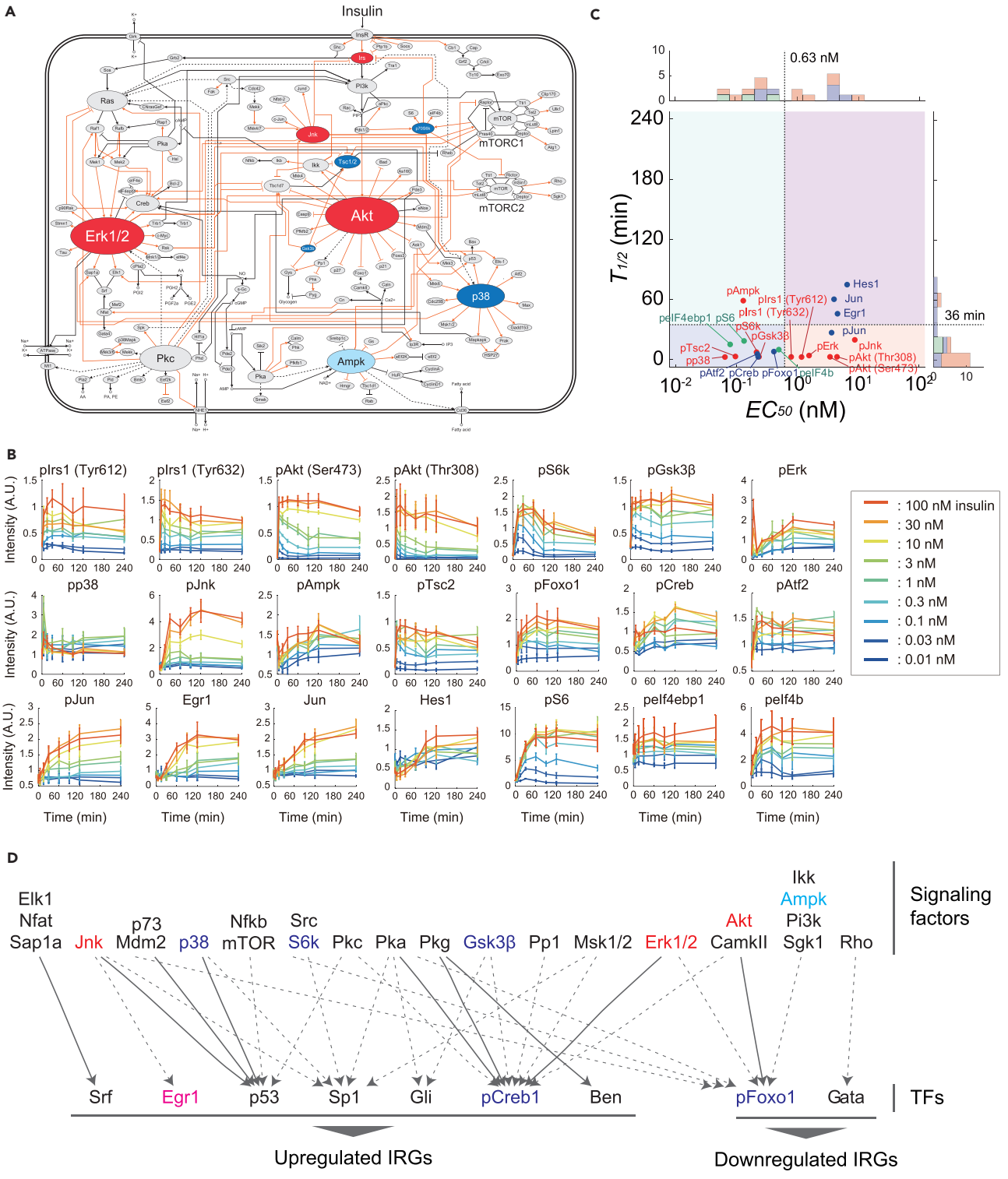

Figure 3. Step II: Connection of TFs and the Signaling Layer

(A) A signaling layer constructed by integrating signaling pathways in which the proteins that exhibited insulin-regulated phosphorylation were significantly over-represented. The colors of the molecules indicate the classes classified by the EC_{50} and $T_{1/2}$ values of the signaling proteins. The size of nodes indicates the number of its interactions with other molecules. Orange edges indicate phosphorylation; black edges, direct interaction; and dashed edges, indirect interaction.

Figure 3. *Continued*

(B) Time courses of the abundance of the signaling proteins in response to the indicated doses of insulin were plotted from data obtained by western blotting (Figure S3C). The means and SEMs of 3 independent experiments are shown. Lowercase "p" preceding the name of a protein indicates the detection of the phosphorylated form of the protein. Numbers and letters in parentheses represent the phosphorylated amino acid residue recognized by the antibody and are numbered according to human proteins.

(C) Distribution of the EC_{50} and $T_{1/2}$ values estimated for the signaling proteins (red), the TFs (blue), and the protein synthesis-related factors (green). Vertical and horizontal dashed lines indicate the thresholds of the EC_{50} and $T_{1/2}$ values, respectively.

(D) The signaling proteins, some of which are TFs (Elk1, Nfat, Sap1a, NF-κB), predicted as upstream regulators of the predicted TFs regulating the IRGs. Black lines indicate regulation of the activity of the TFs included in the signaling layer, and gray dashed lines indicate regulation of the activity of the TFs not included in the signaling layer. The color of the signaling protein reflects its class: dark blue, Class 1; cyan, Class 2; red, Class 3; pink, Class 4.

See also Figures S2 and S3, and Tables S4 and S5.

Focusing on the intra-omic Akt pathway, the EC_{50} and $T_{1/2}$ values for the phosphorylation of Akt place this kinase in the same category as Class 3 IRGs (Table 2), indicating that Akt activity is enhanced by induced insulin stimulation. However, the EC_{50} values of phosphorylated Akt (pAkt) were higher than those of the phosphorylated Akt substrates, phosphorylated Tsc2 (pTsc2), phosphorylated Gsk3β (pGsk3β), and phosphorylated Foxo1 (pFoxo1), and the $T_{1/2}$ value of Akt was almost the same as those of Akt substrates (Figure 3C). The finding of similar $T_{1/2}$ values for Akt and its substrates and lower EC_{50} values for its substrates, which are consistent with a Class 1 response, indicated that Akt rapidly phosphorylates these substrates even in response to basal insulin stimulation and that this kinase responds to basal insulin stimulation to control this intra-omic pathway.

For intra-omic mTOR signaling downstream of Akt in the signaling layer, we evaluated the phosphorylation of eIF4ebp (peIF4ebp), S6K (pS6k), S6 (pS6), and eIF4b (peIF4b), all of which contribute to the activation of translation machinery for protein synthesis. The phosphorylated forms of these proteins exhibited low EC_{50} values and low $T_{1/2}$ values (Table 2), suggesting that basal insulin stimulation promotes protein synthesis through rapid activation of the Akt-mTOR pathway, a finding also consistent with basal insulin stimulation promoting Akt activity (Figures 3C and S3B; Table S5). We measured protein synthesis based on the incorporation of puromycin into newly synthesized proteins (see Methods) and found that the EC_{50} of protein synthesis was 0.035 nM (Figures S3C and S3D), indicating that protein synthesis showed high sensitivity to insulin. The sensitivity and response time analysis of pAkt indicated that this kinase mediates fast responses to induced insulin stimulation, whereas the sensitivity and response time analysis of its substrates and downstream effectors indicated that this kinase mediates the fast response to basal insulin stimulation.

Focusing on the mitogen-activated protein kinase (MAPK) family (Erk, Jnk, and p38), we found that these 3 MAPK families had different sensitivities and response times to insulin stimulation (Figures 3C and S3B; Tables 2 and S5). The insulin-mediated stimulation of pCreb (downstream of Erk) (Vanhoutte et al., 1999) and pAtf (downstream of p38) (Sano et al., 1999) showed high sensitivity and fast response, whereas that of pJun (downstream of pJnk) (Ip and Davis, 1998) showed low sensitivity and fast response. Furthermore, we determined that the total amount of Jun increased in response to induced insulin stimulation (Figure 3C) and that *Jun* was an upregulated IRG of Class 3 (Table S1), indicating that the activity of Jun is regulated by induced insulin stimulation at both the transcriptional (increase in abundance through increased gene expression) and posttranslational (increased phosphorylation) levels, representing intra-omic pathway from the signaling layer to the TF layer and inter-omic pathway from the signaling layer to the TF layer to the IRG layer and back to the TF layer.

Focusing on Hes1 and Egr1, which our analysis indicated are key transcriptional regulators of an intra-omic successive transcriptional cascade, we determined that the change in the abundance of these TFs showed low sensitivity and slow response to insulin. This is consistent with the measured increase in the expression of the encoding genes (Figure 2C and Table S2) at the initial stage and the products subsequently inducing IRGs at a later phase of induced insulin stimulation (Figures 3C and S3B). Many proteins in the signaling layer regulated TFs predicted to control the upregulated IRGs (Figures 3A and 3D). In contrast, only 2 of the 13 TFs that regulated the downregulated IRGs were controlled by proteins in the signaling layer; these were Foxo1, which was connected to 7 kinases in the signaling layer, and Gata, which was connected to the GTPase Rho in the signaling layer (Figures 3A and 3D). With 3 exceptions, the signaling proteins for the TFs controlling the up- and downregulated IRGs did not overlap. The exceptions were the regulation of Foxo1 for downregulated IRGs and Creb1 for upregulated IRGs, both of which are targets of the kinases CamkII,

Akt and Substrates				
	pAkt (Ser473)	pAkt (Thr308)	pGsk3β	pFoxo1
EC_{50} (nM)	3.5	4.5	0.24	0.42
$T_{1/2}$ (min)	2.7	2.7	2.7	8.0
mTOR Substrates and Effectors				
	pS6K	peIF4ebp	pS6	peIF4b
EC_{50} (nM)	0.22	0.079	0.13	0.50
$T_{1/2}$ (min)	7.3	16	20	11
MAPK and Substrates				
	pErk1/2	pCreb	pp38	pAtf1	pJnk	pJun
EC_{50} (nM)	1.2	0.23	0.065	0.22	8.9	3.7
$T_{1/2}$ (min)	2.5	2.7	2.5	5.5	20	27

Table 2. Averages and Medians of EC_{50} and $T_{1/2}$ Values in Insulin-Responsive Kinases and their Substrates

Akt, and Erk1/2. Thus, the FAO cells appeared to use mostly separate signaling factors to regulate distinct sets of TFs that control the up- or downregulated IRGs in response to induced or basal insulin stimulation.

Together with the analysis of transcriptomic data, our observations revealed that cells sensed the different concentrations of insulin and engaged mostly independent pathways to control protein abundance through transcriptional or posttranscriptional mechanisms. Our analysis indicated that basal insulin stimulation activates the translational machinery through an intra-omic Akt-mTOR pathway in the signaling layer and suppresses gene expression through the inter-omic Akt-Foxo1 pathway. Induced insulin stimulation promoted a transcriptional cascade of enhanced gene expression through an inter-omic Erk-IEG pathway. The time constants of protein synthesis-related factors—peIF4ebp, pS6K, pS6, and peIF4b—were much shorter than those of TFs—Hes1 and Egr1 (Figures 3B, 3C, and S3B; Table S5), indicating that basal insulin stimulation quickly promotes protein synthesis without requiring changes in gene expression and induced insulin stimulation promotes a slower transcriptional reprogramming by triggering a successive transcriptional cascade.

Step III: Connection of the IRMs and the IRGs of Metabolic Enzymes

Step III-I: Classification of IRMs by EC_{50} and $T_{1/2}$

Metabolic regulation is an important cellular function of insulin action. KEGG pathway enrichment analysis of IRGs revealed that genes related to metabolism were significantly enriched in the downregulated IRGs (Table S2). Therefore, we measured metabolomic data from FAO cells stimulated with 7 doses of insulin up to 4 hr by capillary electrophoresis-mass spectrometry. We identified 93 IRMs that exhibited significant changes (false discovery rate < 0.1) in response to insulin stimulation using 3-way ANOVA. Using the same criteria that we used for the IRGs (see Methods), we categorized them into 42 increased, 43 decreased, and 8 other IRMs (Figure S4A; Table S6). We then estimated the EC_{50} and $T_{1/2}$ values of the IRMs. The distributions of the EC_{50} values and the $T_{1/2}$ values were significantly different between the increased and decreased IRMs, and the average values of the EC_{50} and the $T_{1/2}$ for the increased IRMs were larger than those for the decreased IRMs (Figure 4A; Table 1). The EC_{50} values of both the increased and decreased IRMs had distinct unimodal distributions with a threshold separating them of 0.40 nM. Most increased IRMs showed low sensitivity, whereas most decreased IRMs showed high sensitivity, indicating that induced insulin stimulation primarily regulated the increased IRMs and basal insulin stimulation regulated the decreased IRMs. The $T_{1/2}$ values of the increased IRMs had a bimodal distribution, whereas those of the decreased IRMs had a unimodal distribution (Figure 4A; Table 1).

Using the thresholds of the EC_{50} and $T_{1/2}$ values, we classified the IRMs into 4 classes (analogous to the classes for the IRGs) and mapped them on KEGG metabolic pathways (Figures 4B and S4B and Table S7). In central carbon metabolism (Figure 4C), the IRMs were divided into 3 functional blocks: (1) a block with

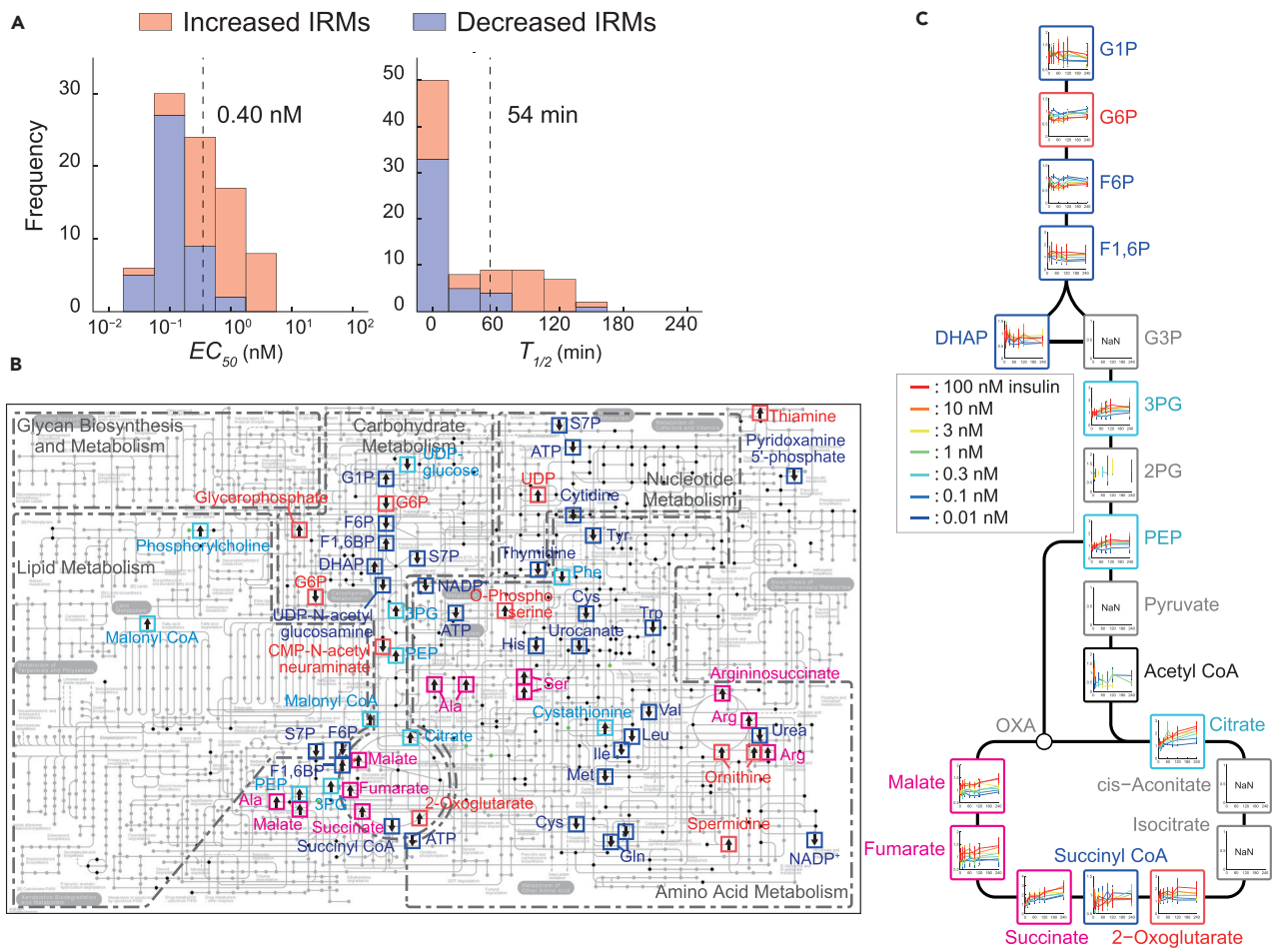
A
Increased IRMs
Decreased IRMs
Frequency
0.40 nM
54 min
EC_{50} (nM)
$T_{1/2}$ (min)
B
Glycan Biosynthesis and Metabolism
Carbohydrate Metabolism
Lipid Metabolism
Nucleotide Metabolism
Amino Acid Metabolism
C
G1P
G6P
F6P
F1,6P
DHAP
G3P
: 100 nM insulin
: 10 nM
: 3 nM
: 1 nM
: 0.3 nM
: 0.1 nM
: 0.01 nM
3PG
2PG
PEP
Pyruvate
Acetyl CoA
OXA
Citrate
Malate
cis−Aconitate
Isocitrate
Fumarate
Succinyl CoA
Succinate
2−Oxoglutarate
D
Upregulated IRGs
High sensitivity
Low sensitivity
Fast response
Fast response
Msmo1 Mat2a
Hmgcr
Downregulated IRGs
High sensitivity
Fast response
Slow response
G6pase Ehhadh Lpin1 B3galt1 Upp2 Ears2
Ppap2b Cyp7a1 Aghphd1 Synj2 Amacr
Baat Inpp4a Cyp8b1 Pklr
Pck1 Rdh16 Cyp2b1
Metabolic enzymes (IRGs)
Glycan Biosynthesis and Metabolism
Lipid Metabolism
Phosphorylcholine
Malonyl CoA
Amino Acid Metabolism
Cys Gln His
Ile Leu Met
Trp Tyr Urea
Val Gly-Gly
Urocanate
Cystathionine Phe
O-Phosphoserine
Ornithine Spermidine
Ala Arg Ser
Argininosuccinate
Nucleotide Metabolism
ATP UDP
Thymidine
Carbohydrate Metabolism
Glycolysis / Gluconeogenesis
DHAP F1,6BP F6P G1P
3PG PEP G6P
TCA cycle
Succinyl CoA
Citrate 2-Oxoglutarate
Fumarate Malate Succinate
Others
UDP-N-acetyl glucosamine
S7P UDP-glucose
CMP-N-acetyl neuraminate
Glycerophosphate
Other
Glutathione(ox) Threonate
S-Lactoylglutathione Cytidine
Pyridoxamine 5'-phosphate
Glycerophosphorylcholine
NADP+ S7P Hydroxyproline
5-Oxoproline Thiamine
IRMs

Figure 4. Step III: Connection of the IRMs and the IRGs of Metabolic Enzymes

(A) Distributions of EC_{50} (left) and $T_{1/2}$ (right) values estimated for the increased IRMs (red bars) and the decreased IRMs (blue bars). To identify a high confidence set of IRMs from multiple experimental datasets, we performed a 3-way ANOVA with the insulin doses, stimulation times, and data acquired on different days as main factors (see Methods).

(B) IRMs projected onto the KEGG *metabolic pathways*. Arrows indicate whether an IRM increased or decreased by insulin stimulation. The colors of the outline and the labels indicate the classes classified by the EC_{50} and $T_{1/2}$ values of the IRMs: dark blue, Class 1; cyan, Class 2; red, Class 3; pink, Class 4.

(C) Metabolites in the central carbon metabolism. The black frames indicate the metabolites that did not show significant changes in response to insulin in a 3-way ANOVA, and gray frames indicate those with unmeasured points at one and more time points (NaN). The other colors correspond to the classes classified by the EC_{50} and $T_{1/2}$ values of IRMs.

(D) The IRGs of metabolic enzymes predicted to regulate the indicated IRMs. The colors of the IRGs and IRMs indicate the classes classified by the EC_{50} and $T_{1/2}$ values.

See also Figure S4, and Tables S6, S7, S8, and S9.

IRMs upstream of glycolysis—glucose-1-phosphate, fructose-6-phosphate, fructose 1,6-bis phosphate, and dihydroxyacetone phosphate—were Class 1 with high sensitivity and fast response times to insulin; (2) a block with IRMs downstream of glycolysis (3-phosphoglycerate and phosphoenolpyruvate) and tricarboxylic acid (TCA) in the TCA cycle (citrate) were all Class 2 with high sensitivity and slow response time; and (3) a block with dicarboxylic acids in TCA cycle—succinate, fumarate, and malate—were Class 4 with low sensitivity and slow response times (Figure 4C). For the IRMs in amino acid metabolism (Figure 4B), those that were decreased by insulin stimulation—Val, Leu, and Ile—were Class 1, indicating that these were regulated by basal insulin stimulation. Those that were increased by insulin stimulation—Ala, Ser, and Arg—are only a few enzymatic steps away from the central carbon metabolism and were Class 4, indicating that induced insulin stimulation regulates the abundance of these amino acids (Figure 4B). Thus, amino acid metabolism was divided into 2 blocks according to the sensitivity and response time to insulin stimulation.

The activities of the metabolic enzymes are regulated by allosteric effectors (activators or inhibitors) that are metabolites (Yugi and Kuroda, 2018; Yugi et al., 2014). We extracted the information of allosteric regulation mediated by IRMs from the BRENDA database and classified the metabolic enzymes regulated by allosteric effectors into 4 classes according to the EC_{50} and the $T_{1/2}$ values of the allosteric effectors (Table S8). Consistent with the changes of the corresponding IRMs (Figure 4B), the IRMs in Class 1 (high sensitivity and fast response) are allosteric effectors that decreased amino acids by promoting their use in glutamate synthesis for entry into the ornithine cycle and the IRMs in Class 4 (low sensitivity and slow response) are allosteric effectors that increase glutamate by inhibiting its entry into the ornithine cycle and the TCA cycle, indicating that basal and induced insulin stimulation regulate amino acid metabolism through different allosteric effectors (Figure S4C).

Step III-II: Connection of the IRGs of Metabolic Enzymes and the IRMs

The last step in building the trans-omic network is connecting the IRGs to the IRMs. We examined the effect of transcriptional regulation on metabolism. We identified 23 IRGs encoding metabolic enzymes, including *G6Pase* and *Pck1* encoding the rate-limiting enzymes in gluconeogenesis (Guo, 2014), *Pklr* encoding a rate-limiting enzyme of glycolysis (Nguyen et al., 2016), *Hmgcr* encoding a rate-limiting enzyme of cholesterol synthesis (Ding et al., 2008), and *Mat2a* encoding a rate-limiting enzyme of methionine metabolism (Kera et al., 2013) (Figures 4D and S4D; Table S9). For gluconeogenesis and glycolysis, *G6Pase* was a Class 1 downregulated IRG and *Pck1* and *Pklr* were Class 2 downregulated IRGs, indicating that the expression of the IRGs encoding the enzymes of gluconeogenesis and glycolysis is reduced in response to basal insulin stimulation. For lipid metabolism, *Hmgcr* was a Class 3 upregulated IRG, *Ehhadh* (encoding a bifunctional enzyme involved in peroxisomal lipid metabolism) was a Class 1 downregulated IRG. For methionine metabolism, *Mat2a* was a Class 1 upregulated IRG. The presence of IRGs encoding rate-limiting enzymes in several metabolic pathways indicated that insulin globally affected metabolism through inter-omic transcriptional regulation.

Step IV: Construction of the Trans-omic Network by Insulin Stimulation

We integrated the networks of Steps I, II, and III and generated the trans-omic network of insulin stimulation starting with transcriptional regulation of IRGs that were connected to TFs through the consensus motifs in the IRG sequences (Figure 5). The TFs were connected to the insulin-responsive signaling proteins in the signaling layer through direct connections (some TFs were in both the inferred TFs from the IRG sequences

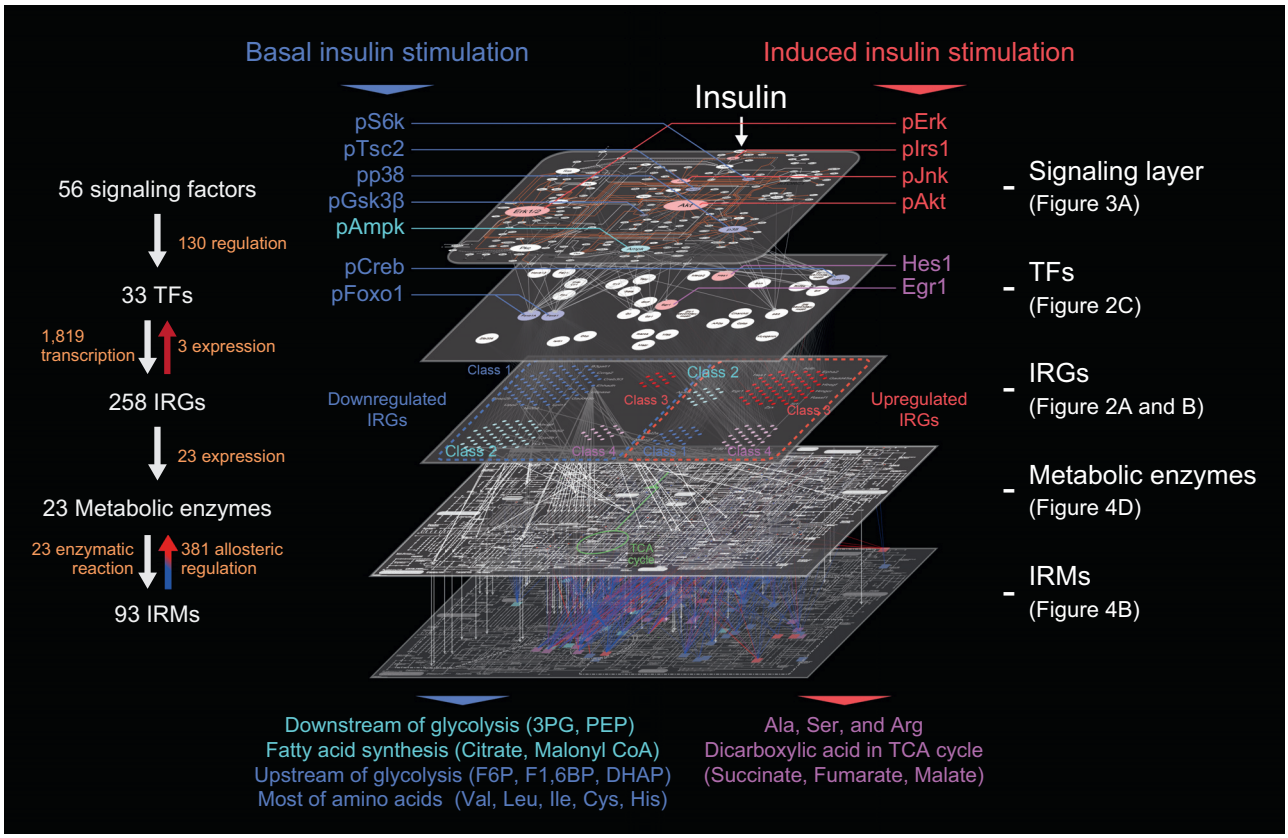

Figure 5. Step IV: Construction of the Trans-omic Network by Insulin Stimulation

The trans-omic network contains 5 layers and the regulatory relationships among them. The colors of molecules and metabolic terms on the trans-omic network indicate the classes classified by the EC_{50} and $T_{1/2}$ values of the IRGs, the same as in Figure 2B. The representative molecules in the selective trans-omic network by induced (right, red) or basal insulin stimulation (left, blue) are shown. See also Figure S5.

and in the signaling layer as proteins that changed in abundance or phosphorylation status in response to insulin) and through inferred connections based on consensus phosphorylation motifs or known interactions with other TFs in the TF layer. Finally, IRMs were connected to the network through the IRGs encoding enzymes involved in their biosynthesis and metabolism. In addition to these 5 layers—signaling, TFs, IRGs, metabolic enzymes, and IRMs—connections between the layers were identified using the IRGs as the anchor. The data used to generate the trans-omic network included information about the dynamics of the response to insulin as well as the sensitivity to insulin, thereby providing a tool for investigating the pathways by which induced and basal insulin signals regulate gene expression and metabolism.

According to sensitivity and time constant, we divided the trans-omic network into the 2 selective trans-omic networks by induced (Figure 5; right, red) and basal (Figure 5; left, blue) insulin stimulation across signaling factors, TFs, IRGs, and IRMs (see Methods), and demonstrated how induced and basal insulin signals are selectively transmitted across the trans-omic network according to the sensitivity of each molecule (Figures 5 and S5). The molecules responding to induced insulin were signaling proteins such as Akt and Erk, which are hub molecules in signaling layer; TFs such as Egr1 and Hes1 (protein expression); and gene expression of the majority of the upregulated IRGs including genes coding TFs. On the other hand, the molecules responding to basal insulin stimulation were signaling molecules related to translational machinery, TFs such as Creb1 and Foxo1 (phosphorylation), gene expression of the majority of the downregulated IRGs including those encoding metabolic enzymes such as *G6pase* and *Pck1*, and IRMs such as most amino acids. One of the selective trans-omic network by induced insulin stimulation was the Erk-dependent successive transcriptional cascade including pCreb, *Egr1*, Egr1, and *Actg1* (Figure S5), whereas that by basal insulin stimulation was the Akt-dependent transcriptional

regulation of metabolism, including pFoxo1, *G6pase*, and G6P (Figure S5). Thus, induced and basal insulin stimulation selectively regulate different sets of signaling proteins, TFs, and genes across the trans-omic network.

Step V: *In Vivo* Validation of Selective Trans-omic Networks by Induced and Basal Insulin Stimulation

We validated the selective trans-omic network by induced and basal insulin stimulation using high (20 μM) and low (2 μM) doses of insulin injection (insulin clamp) in the rat liver (see Methods). By high (20 μM) and low (2 μM) doses of insulin injection, the blood insulin dose reached at 2.5 nM and 0.1 nM around 20 min, respectively, which are consistent with the induced and basal insulin stimulation (Figure 6A). Therefore, we used high (20 μM) and low (2 μM) doses of insulin injection as induced and basal insulin stimulation *in vivo* and measured the time course of signaling factors, TFs, and the IRGs of the rat liver by low and high dose of insulin injection (Figures 6B, 6C, and S6A–S6C). The signaling factors, TFs, and IRGs that significantly changed at more than one time point by both low- and high-dose insulin injection were determined as low-dose insulin-responsive molecules and those that significantly changed only by high-dose insulin injection were determined as high-dose insulin-responsive molecules. Among the 4 molecules included in the selective trans-omic network by basal insulin stimulation (pGsk3β, pS6k, pFoxo1, and pS6), 3 were low-dose insulin-responsive molecules (pGsk3β, pS6k, and pFoxo1) (Figures 6B, 6D, S6A, and S6C). Among the 6 molecules included in the selective trans-omic network by induced insulin stimulation (pAkt [Ser473], pErk, pJun, Hes1, Egr1, and Jun), 3 (pErk, pJun, and Jun) were high-dose insulin-responsive molecules (Figures 6B, 6D, S6A, and S6C). Therefore, 6 of the 10 molecules showed similar sensitivity between FAO cell and rat liver. Note that although pAkt (Ser473), which is included in the selective trans-omic network by induced insulin stimulation, was a low-dose insulin-responsive molecule, the *AUC* in response to high-dose insulin injection was larger than that in response to low-dose insulin injection, indicating that pAkt (Ser473) can effectively discriminate high and low dose of insulin and selectively transmit induced and basal insulin signals. Among the 5 IRGs included in the selective trans-omic network by basal insulin stimulation (*Msmo1*, *Ehhadh*, *G6Pase*, *Pck1*, and *Creb3l2*), 2 (*G6Pase* and *Pck1*) were low-dose insulin-responsive molecules. On the other hand, among the 3 IRGs included in the selective trans-omic network by induced insulin stimulation (*Hmgcr*, *Jun*, *Srf*), none was a high-dose insulin-responsive molecule (Figures 6C, 6D, S6B, and S6C). Therefore, only 2 of the extracted 8 IRGs indicated similar sensitivity in FAO cells and the liver. These differences may be caused from differences of insulin concentration between *in vitro* and *in vivo* experiments.

Taken together, many signaling proteins, TFs, and protein synthesis-related factors, but only part of the IRGs such as *G6pase* and *Pck1* showed similar selectivity by induced and basal insulin stimulation in the insulin-clamped rat liver.

Among the 12 signaling molecules predicted *in vitro*, 6 signaling molecules were confirmed *in vivo* (Figures 6D and 6E). Among the 15 IRGs predicted *in vitro*, 2 IRGs were confirmed *in vivo* (Figures 6D and 6E). Not all of the analyzed proteins or genes exhibited a response to insulin that was consistent with the responses observed in the FAO cells. For responses that were slow in the FAO cells, such as changes that involved intra-omic pathways that stimulated gene expression through the IRG layer, this may reflect complex signal integration *in vivo* resulting from the exposure of the liver to signals other than insulin. Such additional signals may alter either the time course of the response *in vivo* from that in the cultured cells or may change the outcome of the signal. For those responses that involved phosphorylation, events that occur proximally to activation of the insulin receptor, we observed greater consistency between the FAO cells and the insulin-clamped rat livers, suggesting that the intra-omic events in the signaling layer can be accurately classified according to basal or induced insulin responses from the FAO cell data.

DISCUSSION

In this study, we constructed a trans-omic network of insulin action by connecting transcriptomic data, western blotting analysis of signaling proteins, and metabolomic data. We classified each gene, protein, and metabolite into one of 4 classes according to sensitivity and time constant to insulin. Using the trans-omic network and the sensitivity and response time data, we identified pathways mediating induced and basal insulin stimulation both in cultured rat hepatoma cells and in rat liver. Because the induced and basal insulin stimulation represented the "fed" and "fasting" states, our results revealed how these 2 states direct distinct physiological outcomes. We have previously shown that induced and basal insulin

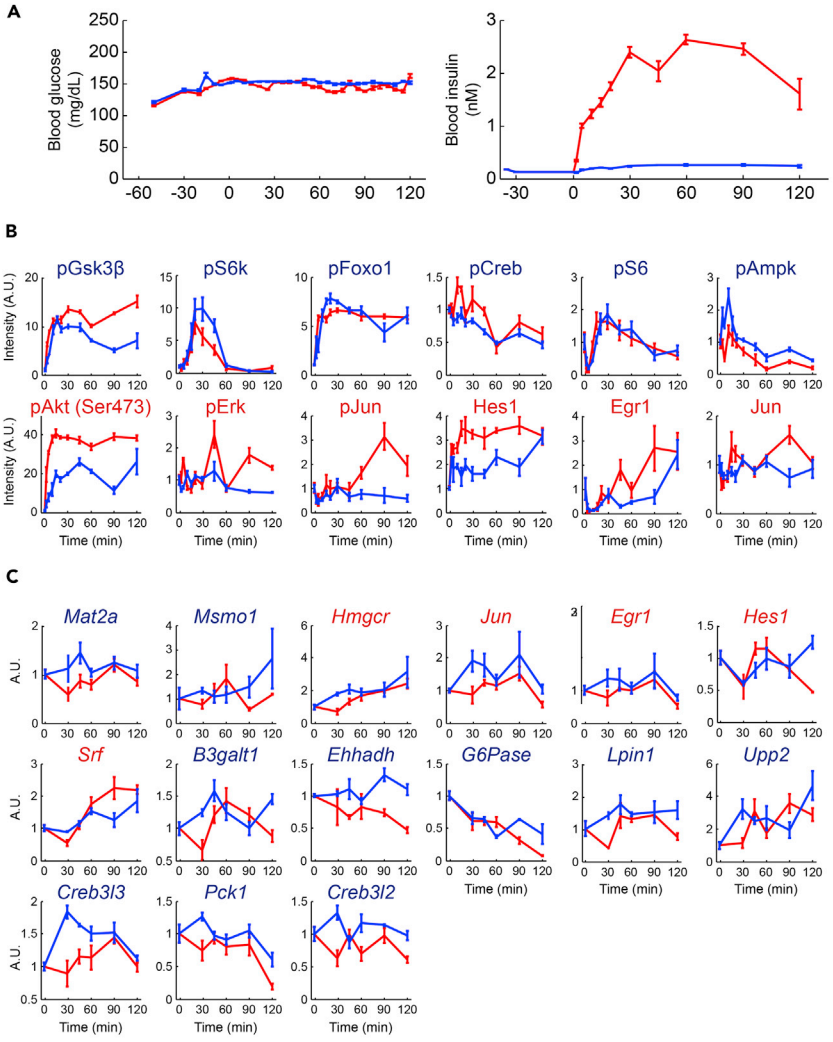

D

		in vitro: Basal insulin stimulation	in vitro: Induced insulin stimulation
in vivo	Low-dose insulin injection	pGsk3b pFoxo1 pS6k	pAkt (Ser473) Hes1
in vivo	High-dose insulin injection		pErk Jun pJun
in vivo	Other	pS6 pCreb pAmpk	Egr1

		in vitro: Basal insulin stimulation	in vitro: Induced insulin stimulation
in vivo	Low-dose insulin injection	*G6Pase Pck1*	*Hmgcr Srf Jun*
in vivo	High-dose insulin injection	*Ehhadh Creb3l2*	
in vivo	Other	*Msmo1 Lpin1 Mat2a Upp2 B3galt1 Creb3l3*	*Egr1 Hes1*

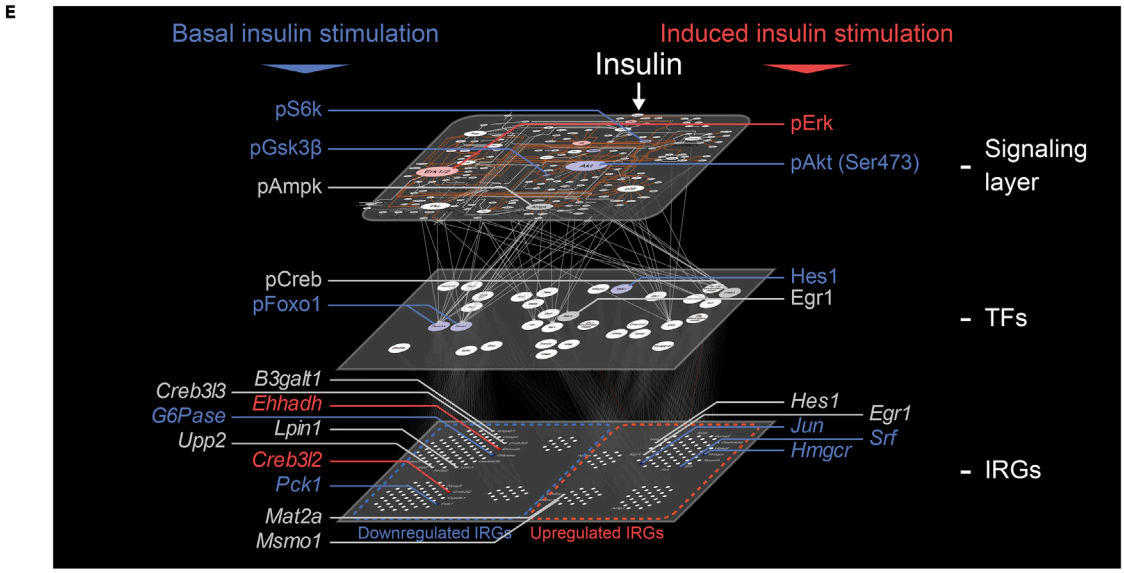

Figure 6. *In Vivo* Validation of Selective Trans-omic Networks by Induced and Basal Insulin Stimulation

(A) Time courses of the concentrations of blood glucose (left) and insulin (right) in response to low-dose (blue) and high-dose (red) insulin injection in rats. The means and SEMs of 3 independent experiments each with 3 animals are shown.

(B) Time courses of the changes in the abundances of the indicated signaling molecules and TFs in rat liver in response to intravenous injection of low-dose (blue) and high-dose (red) insulin. The means and SEMs of 3 independent experiments each with 3 animals are shown. Lowercase "p" preceding the name of a protein indicates the detection of the phosphorylated form of the protein. The y axis indicates relative intensity corrected by the mean of the values at 0 min. The color of the name of the protein indicates the protein responds to induced (red) or basal (blue) insulin stimulation in FAO cells.

(C) Time courses of the expression of the indicated IRGs in rat liver in response to intravenous injection of low dose (blue) and high dose (red) insulin. The means and SEMs of 3 independent experiments each with 3 animals are shown. The y axis indicates relative intensity corrected by mean of the values at 0 min. The color of the name of the protein indicates whether the protein responds to induced (red) or basal (blue) insulin stimulation in FAO cells.

(D) Comparison of the signaling proteins (upper) and IRGs (lower) of the *in vivo* and FAO response to low (basal) and high (induced) concentrations of insulin. Low-dose response *in vivo* indicates that a significant response occurred at more than one time point with a low dose regardless of whether a high dose also stimulated a response. High-dose response only produced a significant response at more than one time point in response to the high dose of insulin. Other indicated the proteins or genes that showed a significant change in response to only low-concentration insulin injection or did not show a significant change. Class designations for the FAO response are based on the EC_{50} and $T_{1/2}$ values. Those proteins or genes with matching rat liver and FAO responses are shaded.

(E) The selective trans-omic network by induced and basal insulin stimulation *in vivo*. The low-dose insulin-responsive molecules (blue), high-dose insulin-responsive molecules (red), and others (gray) are shown.

See also Figure S6, and Tables S10 and S11.

stimulation regulate different physiological functions both in FAO hepatoma cells (Kubota et al., 2012) and in the rat liver (Kubota et al., 2018; Sano et al., 2016). Insulin signals through a single receptor, the insulin receptor; thus, different pathways downstream of insulin receptors are responsible for regulation of the different physiological functions. We used the trans-omic network and kinetic data to identify where such differences emerge in the response to insulin. We found one point of divergence downstream of Akt for high sensitivity to basal insulin stimulation and downstream of Erk for low sensitivity to induced insulin stimulation. In particular, our results indicated that Akt targeted Foxo to control the downregulated IRGs, and Erk targeted a transcriptional cascade mediated through the IEGs to control the upregulated IRGs. These pathways provide a mechanistic explanation for the predominantly downregulated IRG response to basal insulin stimulation and the predominantly upregulated IRG response to induced insulin stimulation that we previously reported (Sano et al., 2016).

Induced and basal insulin stimulation selectively controlled the expression of different gene sets for different functional roles. Our data indicated that through the posttranslational regulation of Foxo proteins by Akt, basal insulin downregulated IRGs. In contrast, induced insulin stimulation controlled the upregulated IRGs through Erk-mediated activation of 2-step transcriptional cascade, initiated by the increased expression of *Hes1*, *Egr1*, and *Srf*, the products of which regulated Classes 3 and 4 upregulated IRGs.

Basal insulin stimulation also phosphorylated the translational machinery through the Akt pathway and increased protein synthesis, indicating that basal insulin stimulation increases protein amount through a general increase in translation, rather than in a transcription-dependent manner. One of the advantages of the translational regulation rather than transcriptional regulation is quickness; it is much faster to increase protein abundance by changing the translation rate of pre-existing mRNA than synthesizing *de novo* mRNA (Brant-Zawadzki et al., 2007). Indeed, all the protein synthesis-related factors we examined showed a fast response to insulin stimulation. Our results indicated that induced and basal insulin stimulation selectively regulate protein abundance through changes in transcription and translation, respectively, and thereby elicit distinct cellular functions during fed and fasting states in different time scales.

We constructed the trans-omic network of insulin action using a combination of data generated in this study (transcriptomic and metabolomic data and, protein data from western blot analysis). We acknowledge that some data and regulatory components required for a comprehensive trans-omic network are not included in the trans-omic network that we constructed. These missing elements include proteome abundance, other types of posttranslational modifications, protein-protein interactions, metabolic flux information, and epigenomic data. Another limitation is that we did not consider synergistic effects among the regulatory components in the trans-omic network. A limitation of the predicted TF-IRG regulatory interactions is that we used a limited genomic region surrounding the consensus transcription start site as the flanking region of each IRG to predict connections to TFs. Other potentially important regions, such as enhancers, were not considered, which means the TF-IRG connections may be

underestimated. In contrast, our attempt to validate the predicted TF-IRG connections using a database of chromatin immunoprecipitation sequencing analysis (ChIP-Atlas) (http://chip-atlas.org) and found that, on average, only 30% of the predicted TFs have been reported to bind to the promoter region of the IRGs (Figure S2). However, the data from rat and liver or hepatic cells were limited in the database. Thus, it remains difficult to construct or validate trans-omic networks using omic datasets available in public databases, because the available data may not match the experimental conditions under which the trans-omic network is tested.

Here, we identified the selective pathways within layers (intra-omic pathways) or between layers (inter-omic pathways) of the trans-omic network that mediate the response to induced or basal insulin stimulation. Furthermore, by integrating sensitivity and response time data, we classified the insulin-responsive component of the trans-omic network according to dynamics and insulin concentration. Future studies can expand the trans-omic network of this study to include other types of data. The methods that we describe for construction of trans-omic networks and integration of sensitivities and time constants of molecules in the trans-omic network enables the exploration of dynamic cellular responses to other stimuli.

METHODS

All methods can be found in the accompanying Transparent Methods supplemental file.

SUPPLEMENTAL INFORMATION

Supplemental Information includes Transparent Methods, 6 figures, 1 scheme, and 11 tables, and can be found with this article online at https://doi.org/10.1016/j.isci.2018.07.022.

ACKNOWLEDGMENTS

We thank our laboratory members for critically reading this manuscript and for their technical assistance with the experiments. The computational analysis of this work was performed in part with support of the super computer system of National Institute of Genetics (NIG), Research Organization of Information and Systems (ROIS). This manuscript was edited by Nancy R. Gough (BioSerendipity, LLC). This work was supported by the Creation of Fundamental Technologies for Understanding and Control of Biosystem Dynamics, CREST (JPMJCR12W3) from the Japan Science and Technology Agency (JST) and by the Japan Society for the Promotion of Science (JSPS) KAKENHI Grant Number (17H06300, 17H06299, 18H03979). K.Y. receives funding from JSPS KAKENHI Grant Number JP15H05582 and JP18H05431, and "Creation of Innovative Technology for Medical Applications Based on the Global Analyses and Regulation of Disease-Related Metabolites", PRESTO (JPMJPR1538) from JST. H.K. was supported by JSPS KAKENHI Grant Number 16H06577. M.F. receives funding from a Grant-in-Aid for Challenging Exploratory Research (16K12508). S.U. receives funding from a Grant-in-Aid for Scientific Research on Innovative Areas (18H04801). K.I.N. and Y.S. were supported by the JSPS KAKENHI Grant Number (17H06301) and (17H06306), respectively. T.S. receives funding from the AMED-CREST (JP18gm0710003) from the Japan Agency for Medical Research and Development, AMED.

AUTHOR CONTRIBUTIONS

K. Kawata, K.Y., A. Hatano, and S.K. conceived the project. K. Kawata, K.Y., A. Hatano, T.K., Y.T., T.S., K.Y.T., M.F., and S.U. analyzed the data. A. Hatano, H.K., and S.K. designed the experiments. A. Hatano performed the western blotting experiments. H.K. performed insulin-clamped rat experiment. M.M. and K.I.N. performed the phosphoproteome measurements. Y.S. performed the RNA-seq experiments. K.S., K. Kato, A.U., M.O., A. Hirayama, and T.S. performed the metabolome measurements. A. Hatano, K. Kawata, K.Y., and S.K. wrote the manuscript.

DECLARATION OF INTERESTS

The authors declare no competing interests.

Received: October 31, 2017
Revised: July 13, 2018
Accepted: July 26, 2018
Published: September 10, 2018

REFERENCES

Biggs, W.H., Meisenhelder, J., Hunter, T., Cavenee, W.K., and Arden, K.C. (1999). Protein kinase B/Akt-mediated phosphorylation promotes nuclear exclusion of the winged helix transcription factor FKHR1. Proc. Natl. Acad. Sci. USA *96*, 7421–7426.

Brabant, G., Prank, K., and Schofl, C. (1992). Pulsatile patterns in hormone secretion. Trends Endocrinol. Metab. *3*, 183–190.

Brant-Zawadzki, P.B., Schmid, D.I., Jiang, H., Weyrich, A.S., Zimmerman, G.A., and Kraiss, L.W. (2007). Translational control in endothelial cells. J. Vasc. Surg. *45* (*Suppl A*), A8–A14.

Brunet, A., Bonni, A., Zigmond, M.J., Lin, M.Z., Juo, P., Hu, L.S., Anderson, M.J., Arden, K.C., Blenis, J., and Greenberg, M.E. (1999). Akt promotes cell survival by phosphorylating and inhibiting a Forkhead transcription factor. Cell *96*, 857–868.

Buescher, J.M., Liebermeister, W., Jules, M., Uhr, M., Muntel, J., Botella, E., Hessling, B., Kleijn, R.J., Le Chat, L., Lecointe, F., et al. (2012). Global network reorganization during dynamic adaptations of bacillus subtilis metabolism. Science *335*, 1099–1103.

Deak, M., Clifton, A.D., Lucocq, L.M., and Alessi, D.R. (1998). Mitogen- and stress-activated protein kinase-1 (MSK1) is directly activated by MAPK and SAPK2/p38, and may mediate activation of CREB. EMBO J. *17*, 4426–4441.

Ding, J., Jiang, D., Kurczy, M., Nalepka, J., Dudley, B., Merkel, E.I., Porter, F.D., Ewing, A.G., Winograd, N., Burgess, J., et al. (2008). Inhibition of HMG CoA reductase reveals an unexpected role for cholesterol during PGC migration in the mouse. BMC Dev. Biol. *8*, 120.

Dupont, J., Khan, J., Qu, B.-H., Metzler, P., Helman, L., and LeRoith, D. (2001). Insulin and IGF-1 Induce different patterns of gene expression in mouse fibroblast NIH-3T3 cells: identification by cDNA microarray analysis. Endocrinology *142*, 4969–4975.

Everman, S., Meyer, C., Tran, L., Hoffman, N., Carroll, C.C., Dedmon, W.L., and Katsanos, C.S. (2016). Insulin does not stimulate muscle protein synthesis during increased plasma branched-chain amino acids alone but still decreases whole body proteolysis in humans. Am. J. Physiol. Endocrinol. Metab. *311*, E671–E677.

Friedman, A.A., Tucker, G., Singh, R., Yan, D., Vinayagam, A., Hu, Y., Binari, R., Hong, P., Sun, X., Porto, M., et al. (2011). Proteomic and functional genomic landscape of receptor tyrosine kinase and ras to extracellular signal-regulated kinase signaling. Sci. Signal. *4*, rs10.

Geiger, R., Rieckmann, J.C., Wolf, T., Basso, C., Feng, Y., Fuhrer, T., Kogadeeva, M., Picotti, P., Meissner, F., Mann, M., et al. (2016). L-arginine modulates t cell metabolism and enhances survival and anti-tumor activity. Cell *167*, 829–842.e13.

Gerosa, L., Haverkorn van Rijsewijk, B.R.B., Christodoulou, D., Kochanowski, K., Schmidt, T.S.B., Noor, E., and Sauer, U. (2015). Pseudo-transition analysis identifies the key regulators of dynamic metabolic adaptations from steady-state data. Cell Syst. *1*, 270–282.

Gonçalves, E., Raguz Nakic, Z., Zampieri, M., Wagih, O., Ochoa, D., Sauer, U., Beltrao, P., and Saez-Rodriguez, J. (2017). Systematic analysis of transcriptional and post-transcriptional regulation of metabolism in yeast. PLoS Comput. Biol. *13*, e1005297.

Gregg, J., and Fraizer, G. (2011). Transcriptional regulation of EGR1 by EGF and the ERK signaling pathway in prostate cancer cells. Genes Cancer *2*, 900–909.

Guo, S. (2014). Insulin signaling, resistance, and the metabolic syndrome: insights from mouse models into disease mechanisms. J. Endocrinol. *220*, T1–T23.

Hackett, S.R., Zanotelli, V.R.T., Xu, W., Goya, J., Park, J.O., Perlman, D.H., Gibney, P.A., Botstein, D., Storey, J.D., and Rabinowitz, J.D. (2016). Systems-level analysis of mechanisms regulating yeast metabolic flux. Science *354*, aaf2786.

Hectors, T.L.M., Vanparys, C., Pereira-Fernandes, A., Knapen, D., and Blust, R. (2012). Mechanistic evaluation of the insulin response in H4IIE hepatoma cells: new endpoints for toxicity testing? Toxicol. Lett. *212*, 180–189.

Humphrey, S., Yang, G., Yang, P., Fazakerley, D., Stöckli, J., Yang, J., and James, D. (2013). Dynamic adipocyte phosphoproteome reveals that Akt directly regulates mTORC2. Cell Metab. *17*, 1009–1020.

Humphrey, S.J., Azimifar, S.B., and Mann, M. (2015). High-throughput phosphoproteomics reveals in vivo insulin signaling dynamics. Nat. Biotechnol. *33*, 990–995.

Ip, Y.T., and Davis, R.J. (1998). Signal transduction by the c-Jun N-terminal kinase (JNK)–from inflammation to development. Curr. Opin. Cell Biol. *10*, 205–219.

Ishii, N., Nakahigashi, K., Baba, T., Robert, M., Soga, T., Kanai, A., Hirasawa, T., Naba, M., Hirai, K., Hoque, A., et al. (2007). Multiple high-throughput analyses monitor the response of *E. coli* to perturbations. Science *316*, 593–597.

Jastrzebski, K., Hannan, K.M., Tchoubrieva, E.B., Hannan, R.D., and Pearson, R.B. (2007). Coordinate regulation of ribosome biogenesis and function by the ribosomal protein S6 kinase, a key mediator of mTOR function. Growth Factors *25*, 209–226.

Kera, Y., Katoh, Y., Ohta, M., Matsumoto, M., Takano-Yamamoto, T., and Igarashi, K. (2013). Methionine adenosyltransferase ii-dependent histone H3K9 methylation at the *COX-2* gene locus. J. Biol. Chem. *288*, 13592–13601.

Kim, H.S., and Lee, N.K. (2014). Gene expression profiling in osteoclast precursors by insulin using microarray analysis. Mol. Cells *37*, 827–832.

Krüger, M., Kratchmarova, I., Blagoev, B., Tseng, Y.-H., Kahn, C.R., and Mann, M. (2008). Dissection of the insulin signaling pathway via quantitative phosphoproteomics. Proc. Natl. Acad. Sci. USA *105*, 2451–2456.

Kubota, H., Noguchi, R., Toyoshima, Y., Ozaki, Y., Uda, S., Watanabe, K., Ogawa, W., and Kuroda, S. (2012). Temporal coding of insulin action through multiplexing of the AKT pathway. Mol. Cell *46*, 820–832.

Kubota, H., Uda, S., Matsuzaki, F., Yamauchi, Y., and Kuroda, S. (2018). In vivo decoding mechanisms of the temporal patterns of blood insulin by the insulin-AKT pathway in the liver. Cell Syst. *7*, 118–128.e3.

Lindsay, J.R., McKillop, A.M., Mooney, M.H., Flatt, P.R., Bell, P.M., and O'Harte, F.P.M. (2003). Meal-induced 24-hour profile of circulating glycated insulin in type 2 diabetic subjects measured by a novel radioimmunoassay. Metabolism *52*, 631–635.

Lizcano, J.M., and Alessi, D.R. (2002). The insulin signalling pathway. Curr. Biol. *12*, R236–R238.

Monetti, M., Nagaraj, N., Sharma, K., and Mann, M. (2011). Large-scale phosphosite quantification in tissues by a spike-in SILAC method. Nat. Methods *8*, 655–658.

Murphy, L.O., MacKeigan, J.P., and Blenis, J. (2004). A network of immediate early gene products propagates subtle differences in mitogen-activated protein kinase signal amplitude and duration. Mol. Cell. Biol. *24*, 144–153.

Nakayama, K., Satoh, T., Igari, A., Kageyama, R., and Nishida, E. (2008). FGF induces oscillations of Hes1 expression and Ras/ERK activation. Curr. Biol. *18*, R332–R334.

Nguyen, A., Loo, J.M., Mital, R., Weinberg, E.M., Man, F.Y., Zeng, Z., Paty, P.B., Saltz, L., Janjigian, Y.Y., de Stanchina, E., et al. (2016). PKLR promotes colorectal cancer liver colonization through induction of glutathione synthesis. J. Clin. Invest. *126*, 681–694.

Noguchi, R., Kubota, H., Yugi, K., Toyoshima, Y., Komori, Y., Soga, T., and Kuroda, S. (2013). The selective control of glycolysis, gluconeogenesis and glycogenesis by temporal insulin patterns. Mol. Syst. Biol. *9*, 664.

O'Meara, N.M., Sturis, J., Blackman, J.D., Roland, D.C., Van Cauter, E., and Polonsky, K.S. (1993). Analytical problems in detecting rapid insulin secretory pulses in normal humans. Am. J. Physiol. *264*, E231–E238.

O'Rahilly, S., Turner, R.C., and Matthews, D.R. (1988). Impaired pulsatile secretion of insulin in relatives of patients with non-insulin-dependent diabetes. N. Engl. J. Med. *318*, 1225–1230.

Oliveira, A.P., Ludwig, C., Picotti, P., Kogadeeva, M., Aebersold, R., and Sauer, U. (2012). Regulation of yeast central metabolism by enzyme phosphorylation. Mol. Syst. Biol. *8*, 623.

Otsu, N. (1979). A threshold selection method from gray-level histograms. IEEE Trans. Syst. Man. Cybern. *9*, 62–66.

Polonsky, K.S., Given, B.D., and Van Cauter, E. (1988). Twenty-four-hour profiles and pulsatile patterns of insulin secretion in normal and obese subjects. J. Clin. Invest. *81*, 442–448.

Rome, S., Clément, K., Rabasa-Lhoret, R., Loizon, E., Poitou, C., Barsh, G.S., Riou, J.-P., Laville, M., and Vidal, H. (2003). Microarray profiling of human skeletal muscle reveals that insulin regulates approximately 800 genes during a hyperinsulinemic clamp. J. Biol. Chem. *278*, 18063–18068.

Saltiel, A.R., and Kahn, C.R. (2001). Insulin signalling and the regulation of glucose and lipid metabolism. Nature *414*, 799–806.

Sano, T., Kawata, K., Ohno, S., Yugi, K., Kakuda, H., Kubota, H., Uda, S., Fujii, M., Kunida, K., Hoshino, D., et al. (2016). Selective control of up-regulated and down-regulated genes by temporal patterns and doses of insulin. Sci. Signal. *112*, 1–12.

Sano, Y., Harada, J., Tashiro, S., Gotoh-Mandeville, R., Maekawa, T., and Ishii, S. (1999). ATF-2 is a common nuclear target of Smad and TAK1 pathways in transforming growth factor-beta signaling. J. Biol. Chem. *274*, 8949–8957.

Shaul, Y.D., and Seger, R. (2007). The MEK/ERK cascade: from signaling specificity to diverse functions. Biochim. Biophys. Acta *1773*, 1213–1226.

Titchenell, P.M., Lazar, M.A., and Birnbaum, M.J. (2017). Unraveling the regulation of hepatic metabolism by insulin. Trends Endocrinol. Metab. *28*, 497–505.

Vanhoutte, P., Barnier, J.V., Guibert, B., Pagès, C., Besson, M.J., Hipskind, R.A., and Caboche, J. (1999). Glutamate induces phosphorylation of Elk-1 and CREB, along with c-fos activation, via an extracellular signal-regulated kinase-dependent pathway in brain slices. Mol. Cell. Biol. *19*, 136–146.

Versteyhe, S., Klaproth, B., Borup, R., Palsgaard, J., Jensen, M., Gray, S.G., and De Meyts, P. (2013). IGF-I, IGF-ii, and insulin stimulate different gene expression responses through binding to the IGF-I receptor. Front. Endocrinol. (Lausanne) *4*, 98.

Vinayagam, A., Kulkarni, M.M., Sopko, R., Sun, X., Hu, Y., Nand, A., Villalta, C., Moghimi, A., Yang, X., Mohr, S.E., et al. (2016). An integrative analysis of the InR/PI3K/Akt network identifies the dynamic response to insulin signaling. Cell Rep. *16*, 3062–3074.

Whiteman, E.L., Cho, H., and Birnbaum, M.J. (2002). Role of Akt/protein kinase B in metabolism. Trends Endocrinol. Metab. *13*, 444–451.

Yugi, K., and Kuroda, S. (2017). Metabolism-centric trans-omics. Cell Syst. *4*, 19–20.

Yugi, K., and Kuroda, S. (2018). Metabolism as a signal generator across trans-omic networks at distinct time scales. Curr. Opin. Syst. Biol. *8*, 59–66.

Yugi, K., Kubota, H., Toyoshima, Y., Noguchi, R., Kawata, K., Komori, Y., Uda, S., Kunida, K., Tomizawa, Y., Funato, Y., et al. (2014). Reconstruction of insulin signal flow from phosphoproteome and metabolome data. Cell Rep. *8*, 1171–1183.

Yugi, K., Kubota, H., Hatano, A., and Kuroda, S. (2016). Trans-omics: how to reconstruct biochemical networks across multiple'omic' layers. Trends Biotechnol. *34*, 276–290.

Yusufi, F.N.K., Lakshmanan, M., Ho, Y.S., Loo, B.L.W., Ariyaratne, P., Yang, Y., Ng, S.K., Tan, T.R.M., Yeo, H.C., Lim, H.L., et al. (2017). Mammalian systems biotechnology reveals global cellular adaptations in a recombinant CHO cell line. Cell Syst. *4*, 530–542.e6.

Zhang, Y., Zhang, Y., and Yu, Y. (2017). Global phosphoproteomic analysis of insulin/akt/mTORC1/S6K signaling in rat hepatocytes. J. Proteome Res. https://doi.org/10.1021/acs.jproteome.7b00140.

Zimmet, P., Alberti, K.G.M.M., and Shaw, J. (2001). Global and societal implications of the diabetes epidemic. Nature *414*, 782–787.

ISCI, Volume 7

Supplemental Information

Trans-omic Analysis Reveals Selective Responses to Induced and Basal Insulin across Signaling, Transcriptional, and Metabolic Networks

Kentaro Kawata, Atsushi Hatano, Katsuyuki Yugi, Hiroyuki Kubota, Takanori Sano, Masashi Fujii, Yoko Tomizawa, Toshiya Kokaji, Kaori Y. Tanaka, Shinsuke Uda, Yutaka Suzuki, Masaki Matsumoto, Keiichi I. Nakayama, Kaori Saitoh, Keiko Kato, Ayano Ueno, Maki Ohishi, Akiyoshi Hirayama, Tomoyoshi Soga, and Shinya Kuroda

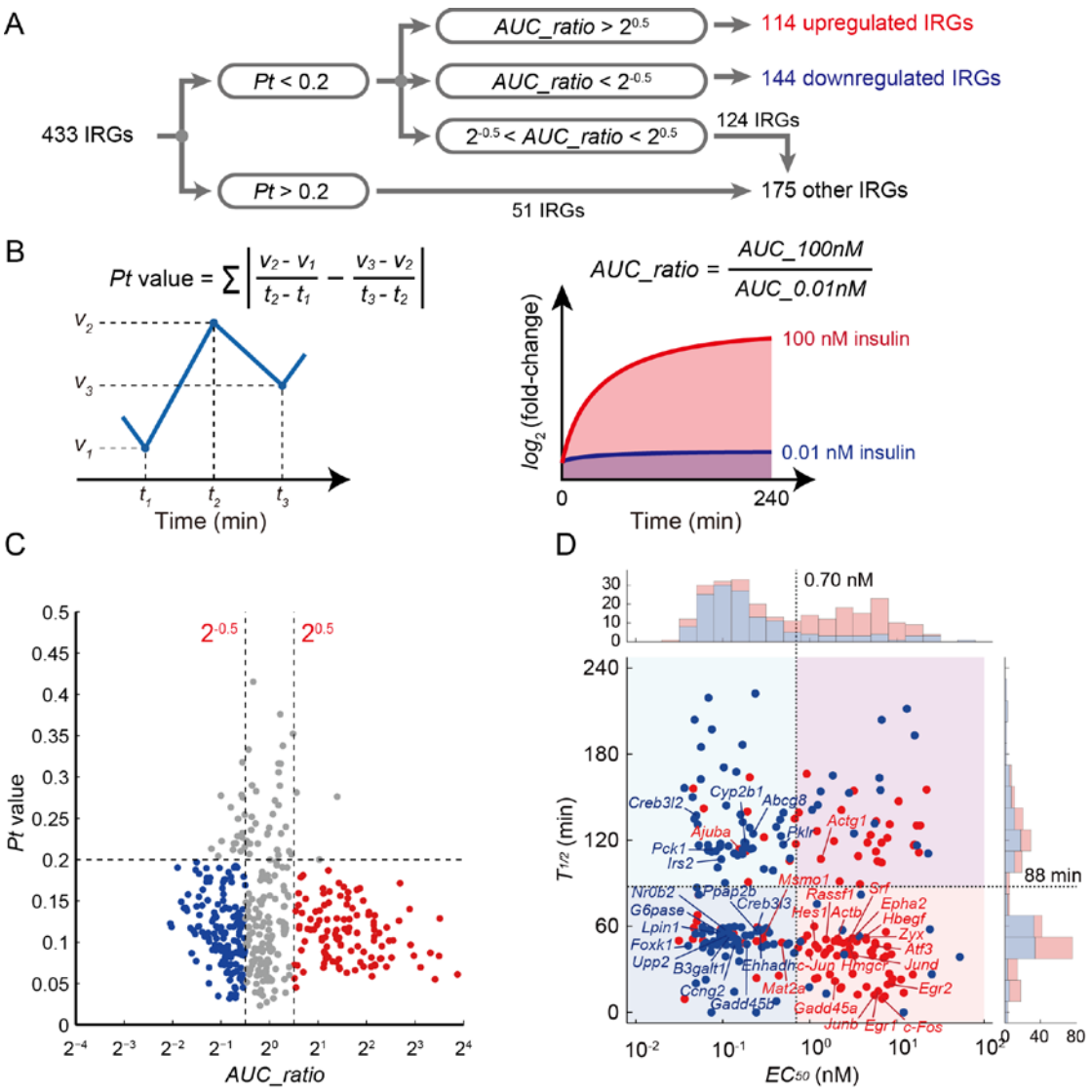

Figure S1. Classification of IRGs according to insulin sensitivity and response time, Related to Figure 2. (A) Definition of the upregulated and downregulated IRGs. (B) Definition of *Pt* value, an index of expression variation (left), and *AUC_ratio*, an index of response (right). (C) Distribution of *Pt* values and *AUC_ratio*s in the upregulated IRGs (red dots) and downregulated IRGs (blue dots). Gray dots indicate the IRGs defined as neither upregulated nor downregulated IRGs. Horizontal and vertical dashed lines indicate thresholds of *Pt* values and *AUC_ratio*s, respectively. (D) Distribution of the EC_{50} and $T_{1/2}$ values estimated for the upregulated (red dots) and downregulated IRGs (blue dots). Vertical and horizontal dashed lines indicate the thresholds of the EC_{50} and $T_{1/2}$ values, respectively.

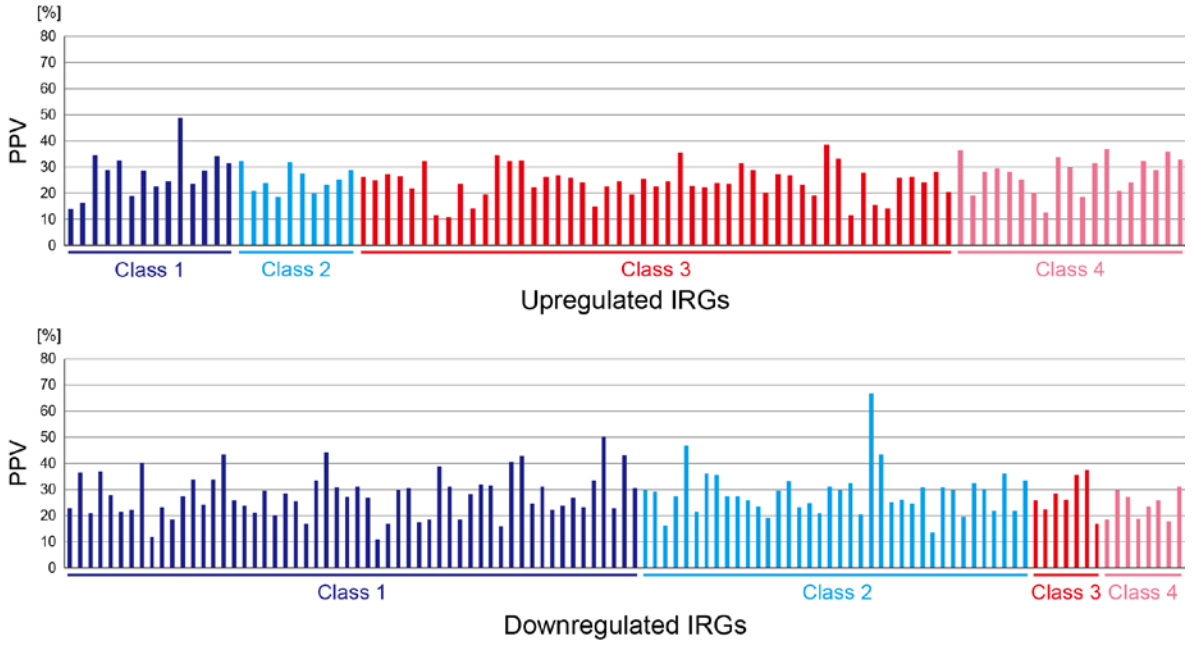

Figure S2. Positive predictive values of the predicted TFs, Related to Figure 2. We validated the matching of TFs to IRGs with ChIP-Atlas (http://chip-atlas.org), which is a database of chromatin immunoprecipitation sequencing (ChIP-seq) data. We used ChIP-seq data related to mouse transcription factors, instead of rat transcription factors, because the available rat data was too limited. Extracted data from ChIP-Atlas were not limited to only liver or hepatocytes. We regarded the TFs identified for each IRG from ChIP-Atlas as positive examples. We calculated positive predictive values (PPVs) of the predicted TFs for each IRG. The PPV was calculated for each upregulated (upper) and downregulated IRG (lower) from the frequency of occurrence of the predicted TF at the IRG in ChIP-seq data

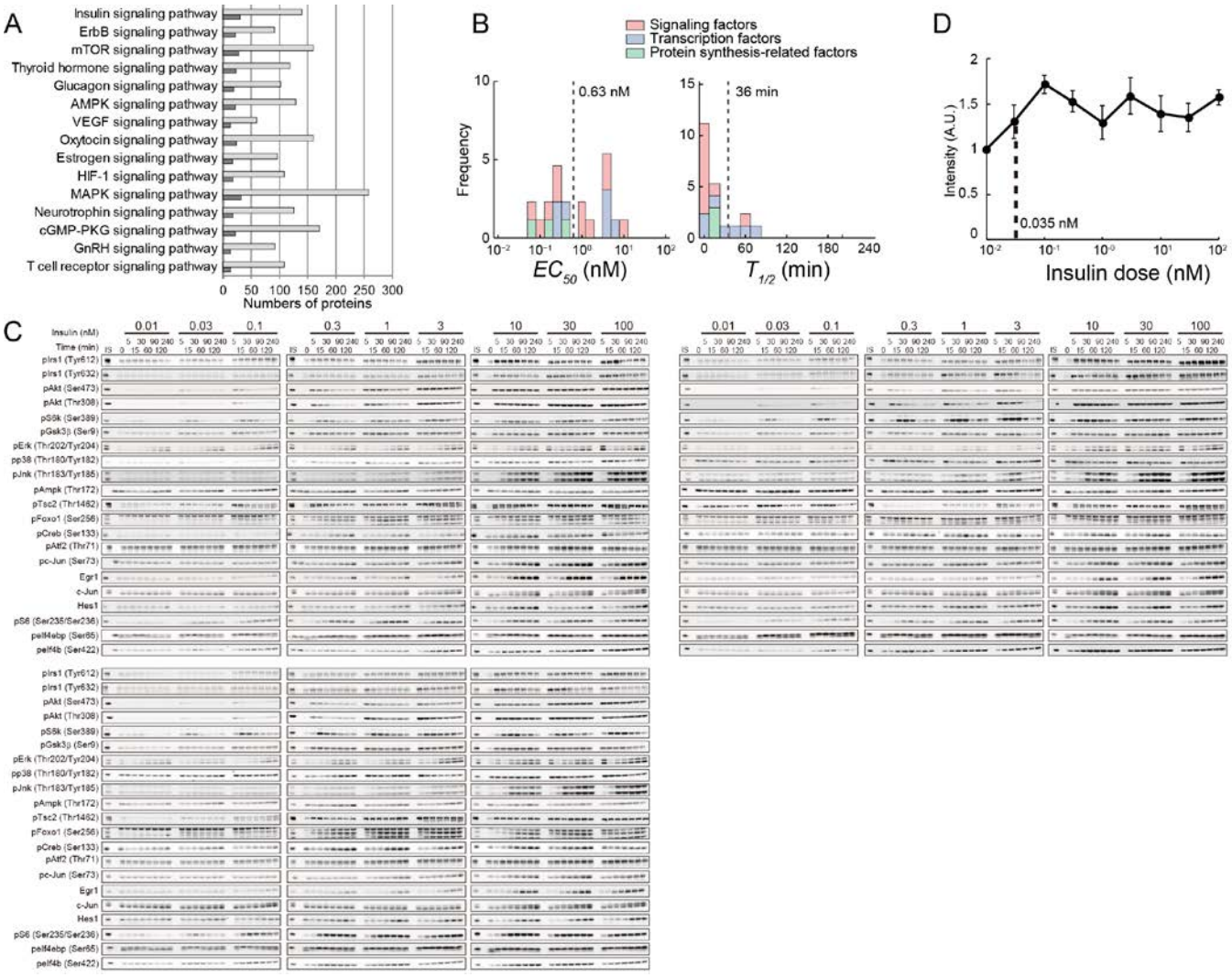

Figure S3. Classification of the signaling proteins, TFs and protein synthesis-related factors, according to insulin sensitivity and response time, Related to Figure 3. (A) Number of the proteins in the KEGG signaling pathways. The light gray bars indicate the total numbers of proteins and the dark gray bars indicate the numbers of phosphoprotein included in each signaling pathway. (B) Distribution of the EC_{50} and $T_{1/2}$ values estimated for the signaling proteins (red), the TFs (blue), and the protein synthesis-related factors (green). Dashed lines indicate the thresholds of the EC_{50} (left) and $T_{1/2}$ (right) values. (C) All Western blot data for three independent experiments are shown. IS indicates internal standard. Antibodies recognized the indicated protein or protein phosphorylated at the residues indicate. Residue number is human. (D) Relative amount of new protein synthesis based on the incorporation of puromycin into newly synthesized proteins at the indicated dose of insulin stimulation. Data are normalized to those at 0.01 nM insulin stimulation. The means and SEMs of four independent experiments are shown. Dashed line indicates the EC_{50} value.

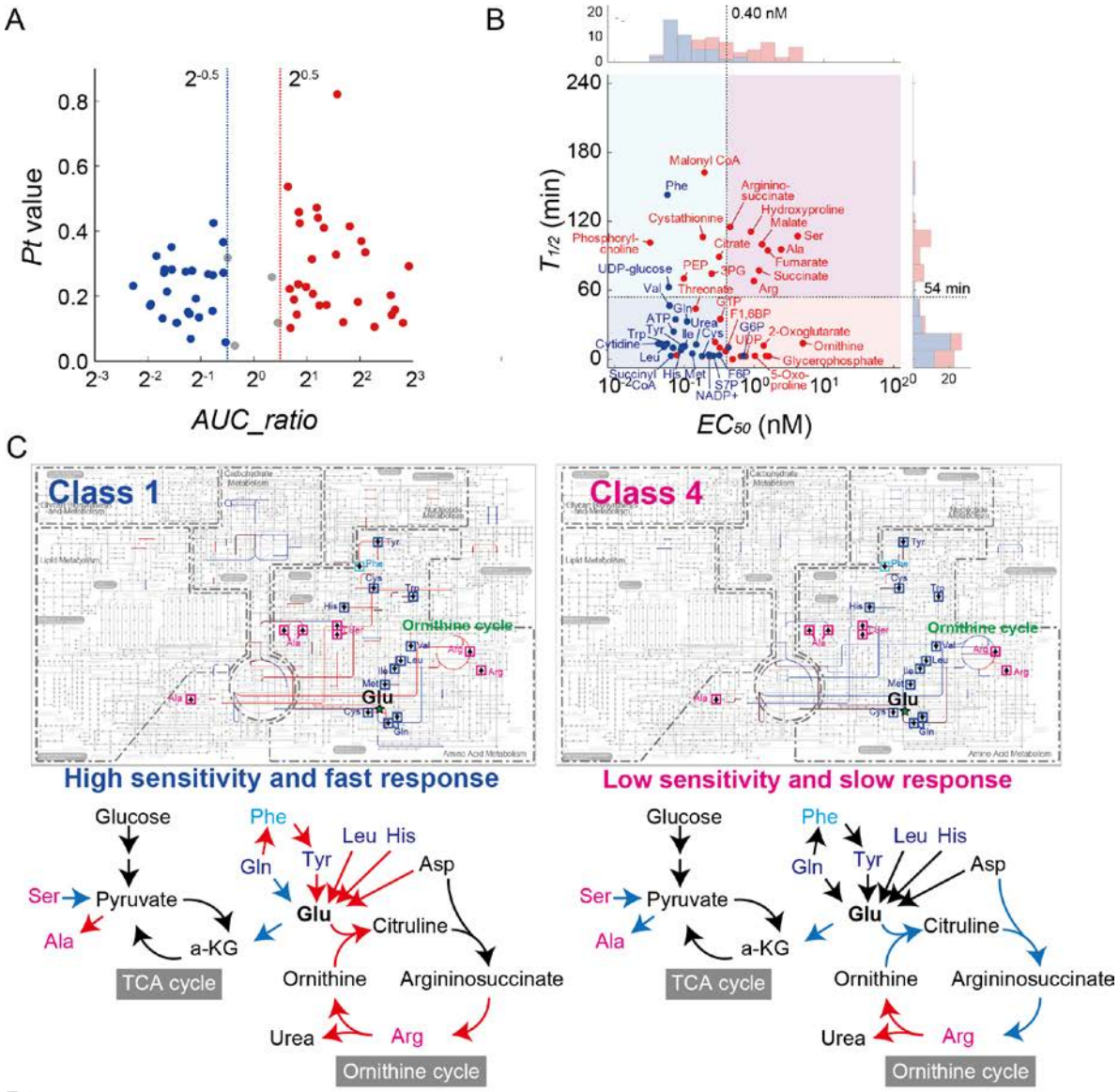
A
Pt value
AUC_ratio
2-0.5
20.5
B
0.40 nM
T1/2 (min)
54 min
EC50 (nM)
Malonyl CoA
Phe
Arginino-succinate
Hydroxyproline
Cystathionine
Malate
Phosphoryl-choline
Citrate
Ser
Ala
UDP-glucose
PEP
3PG
Fumarate
Succinate
Val
Threonate
Arg
Gln
GTP
ATP
Urea
F1,6BP
Trp
Tyr
Ile/Cys
G6P
2-Oxoglutarate
Cytidine
UDP
Ornithine
Leu
Glycerophosphate
Succinyl-CoA
His
Met
S7P
NADP+
F6P
5-Oxo-proline
C
Class 1
Class 4
Ornithine cycle
Glu
High sensitivity and fast response
Low sensitivity and slow response
Glucose
Pyruvate
Ser
Ala
a-KG
TCA cycle
Phe
Leu
His
Gln
Tyr
Asp
Citruline
Ornithine
Argininosuccinate
Urea
Arg
Ornithine cycle
D
Carbohydrate Metabolism
Glycan Biosynthesis and Metabolism
Lipid Metabolism
Nucleotide Metabolism
Amino Acid Metabolism
B3galt1↓
G6pase↓
Lpin1↓
Ppap2b1↓
Cyp2b1↓
Rdh16↓
Sunj2↓
Inpp4a↓
Pklr↓
Upp2↓
Baat↓
Pck1↓
Ehhadh↓
Ears2↓
Agphd1↓
Msmo1↑
Hmgcr↑
Dmnt1
Mat2a↑
Lap3
Syp8b1↓
Syp7b1↓
Amacr↓

Figure S4. Classification of the IRMs according to insulin sensitivity and response time, Related to Figure 4. (A) Distribution of *Pt* values and *AUC_ratio*s in the increased IRMs (red dots) and decreased IRMs (blue dots). Gray dots indicate the IRMs defined as neither increased nor decreased. Vertical dashed lines indicate the threshold of *AUC_ratio*s. (B) Distribution of the EC_{50} and $T_{1/2}$ values calculated for the IRMs. Vertical and horizontal dashed lines indicate the thresholds of the EC_{50} and $T_{1/2}$ values, respectively. (C) Allosteric regulation by the allosteric effectors in Class 1 and Class 4 in Figure S2B projected onto the KEGG *metabolic pathways* (upper) and schemes (lower). Arrows on the KEGG *metabolic pathways* indicate whether an IRM increased or decreased by insulin stimulation. The colors of the box outlines and the labels indicate the classes classified by the EC_{50} and $T_{1/2}$ values of the IRMs: Dark blue, Class 1; cyan, Class 2; red, Class 3; magenta, Class 4. In the schemes, the reactions regulated by allosteric effectors were colored in red (activation), blue (inhibition), and black (not regulated). The IRM text color indicated the classes of the IRMs in the schemes. Because the activities of the metabolic enzymes are regulated by allosteric effectors (activators or inhibitors) that are metabolites, such effectors that are IRMs and change in response to insulin stimulation is a key modulatory mechanism of the metabolic network (Yugi and Kuroda, 2018; Yugi et al., 2014). Therefore, we extracted the information of allosteric regulation mediated by the IRMs from BRENDA database, and classified the allosteric regulation into four classes according to the EC_{50} and the $T_{1/2}$ values of allosteric effectors and mapped to KEGG metabolic pathway. We identified marked changes of allosteric regulation related to amino acid degradation pathway. For Class1, the pathways related to amino acids degradation and ornithine cycle were activated. These results were supported by fast decrease in most of the amino acids in response to basal insulin stimulation. For Class4, glutamate dehydrogenase and ornithine cycle were inhibited. (D) Enzymatic reactions of metabolic enzymes encoded by IRGs projected on the KEGG *metabolic pathways*. Arrows indicate whether an IRG increased or decreased by insulin stimulation. IRG text color indicates the Class of the IRGs, and reactions are colored to match the class of the associated IRG: blue, Class 1; cyan, Class 2; red, Class 3; green, IRGs not included in upregulated or downregulated IRGs.

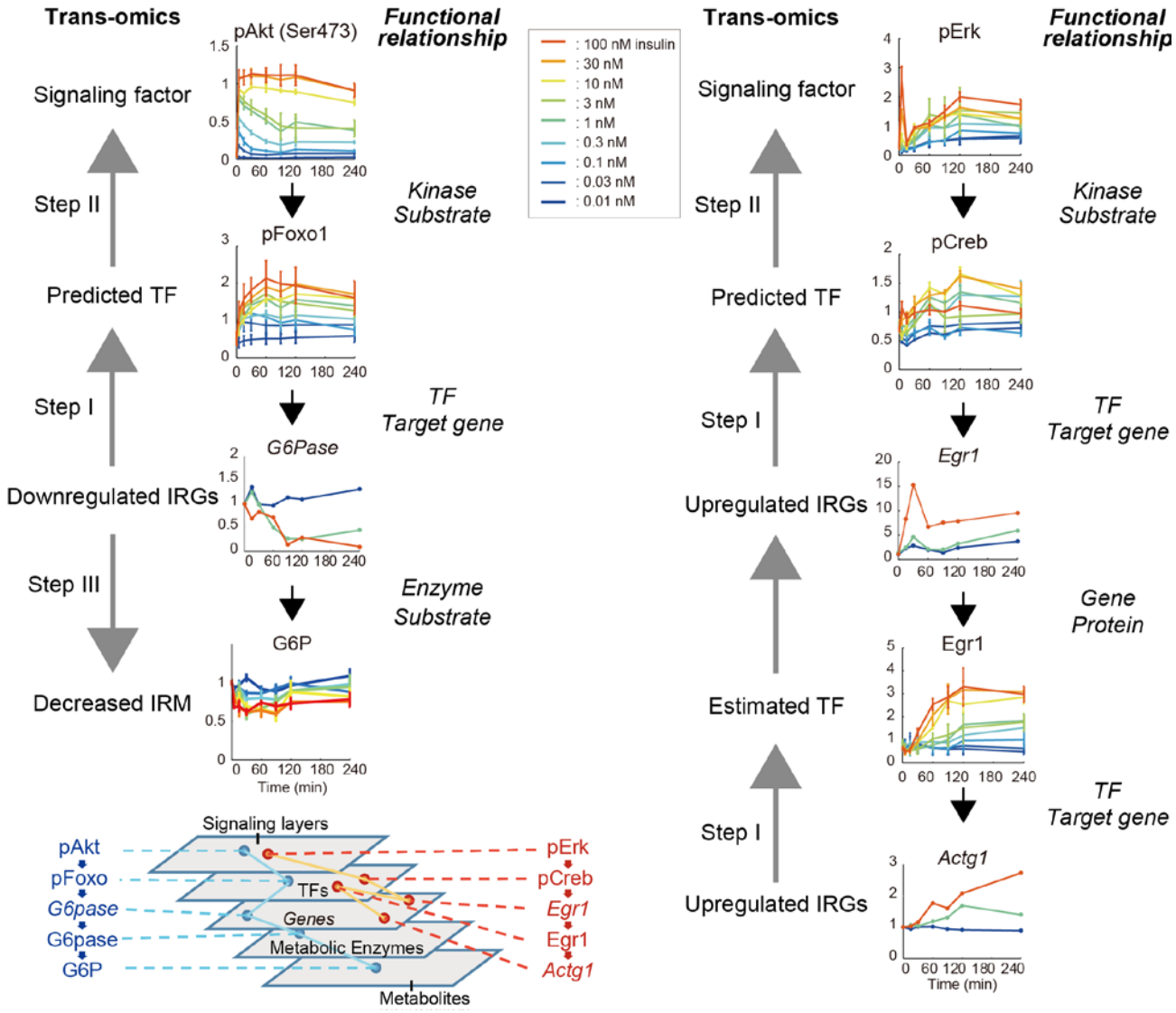

Figure S5. Representative pathways of the selective trans-omic network, Related to Figure 6.

Akt-Foxo-downregulated genes (left) and Erk-IEG-upregulated genes (right), as representative pathways of the selective trans-omic network by basal and induced insulin stimulation, respectively. The molecules in Akt-Foxo-downregulated genes pathway, including Akt (signaling factor), Foxo1 (TF), *G6pase* (gene) and G6P (metabolite) pathway respond to basal insulin stimulation. The majority of molecules in Erk-IEG-upregulated genes pathway, including Erk (signaling factor), Creb (TF), *Egr1* (gene), Egr1 (TF) and *Actg1* (gene) pathway respond to induced insulin stimulation. "Trans-omics" indicates the steps for integration of two layers in Figure 1B. "Functional relationship" indicates the relationship between molecules in biological function.

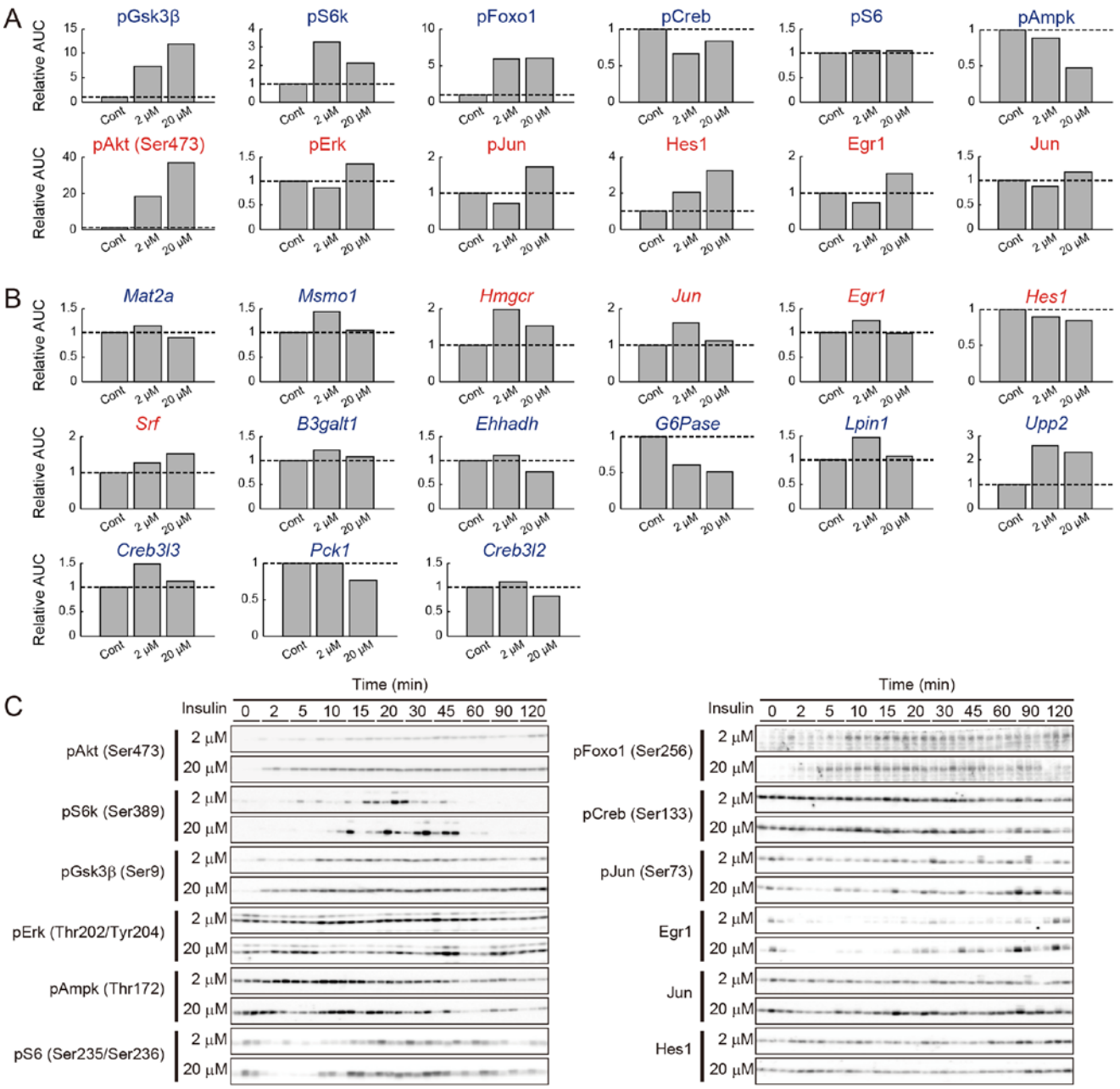

Figure S6. *in vivo* Validation of the selective trans-omic network by high- and low-doses of insulin injection, Related to Figure 6. (A) *AUC*s calculated from the time courses of mean intensities in response to each dose of insulin injected. *AUC*s in response to 2 and 20 μM insulin injection were normalized by those with the mean intensities without insulin injection. (B) *AUC*s calculated from the time courses of mean relative expression in response to each dose of insulin injected. The *AUC*s in response to 2 and 20 μM insulin injection were normalized by those with the mean relative expression without insulin injection. In A and B, an *AUC* above the uninjected sample indicates an increase in abundance; an *AUC* below the uninjected sample indicates a decrease in abundance. Text color indicates if the protein or gene responded to basal or induced insulin signaling in FAO cells. (C) All Western blot data are shown.

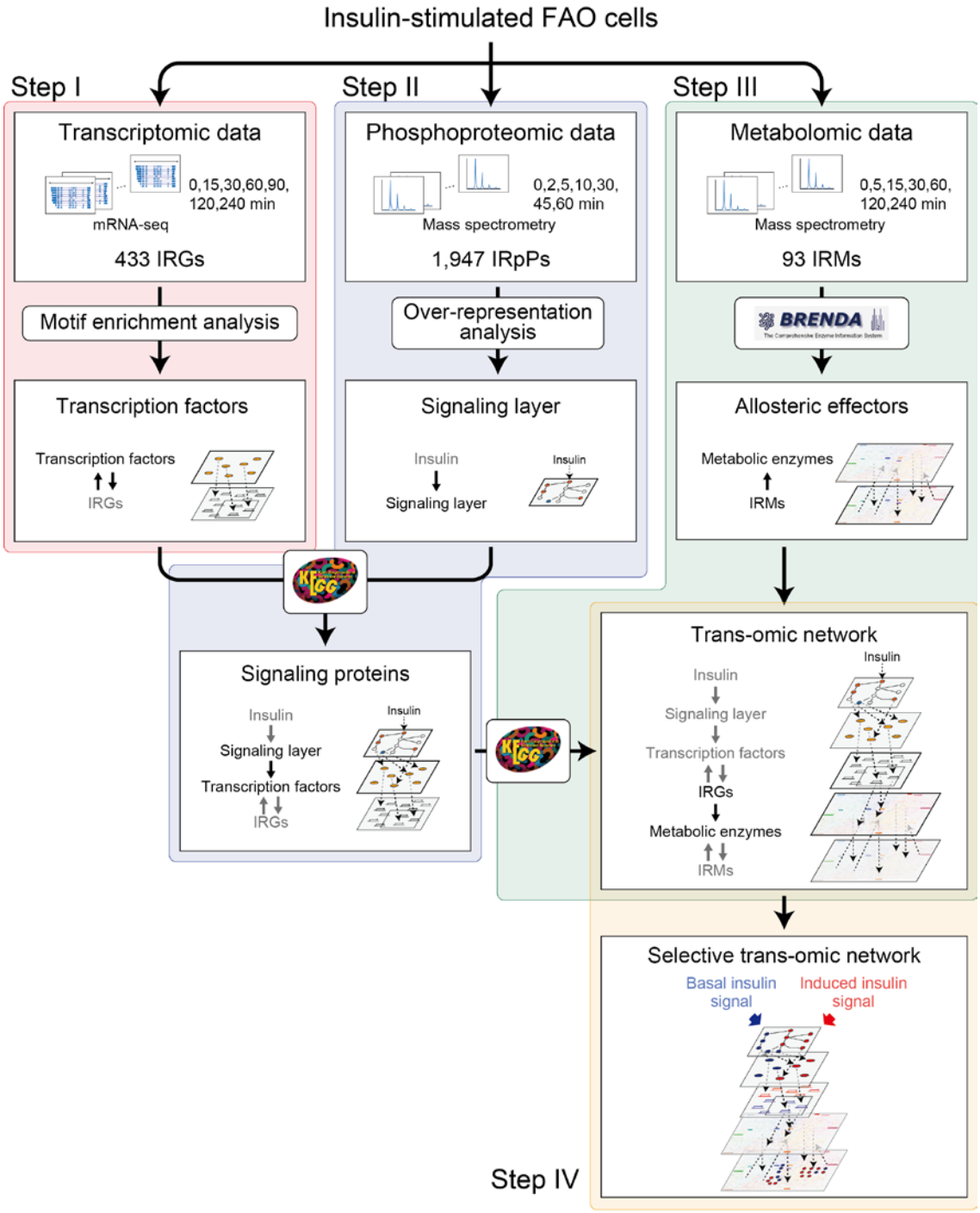

Scheme S1. Scheme of procedures for trans-omic network construction, Related to Figure 1. The trans-omic network was constructed in four main steps (Step I-IV) by defining five layers based on phosphoproteomic, transcriptomic, and metabolomic data, and connecting between the layers. The detailed procedures can be found in Methods.

Table S1. Classification of insulin-responsive genes (IRGs), Related to Figure 2.

Table S2. Enrichment analysis of IRGs classified according to the sensitivity and time constants, Related to Figure 2.

Table S3. Prediction of transcription factors (TFs) for each class of IRGs, Related to Figure 2.

Table S4. Pathway over-representation analysis using insulin-responsive phophoproteins (IRpPs), Related to Figure 3.

Table S5. Classification of signaling proteins, transcription factor, and protein-synthesis related factors, Related to Figure 3

Name	Function	EC_{50} (nM)	$T_{1/2}$ (min)	Class
pGsk3β	Signaling protein	0.2362	2.7308	Class 1
pp38	Signaling protein	0.0649	2.5000	Class 1
pS6k	Signaling protein	0.2158	7.2863	Class 1
pTsc2	Signaling protein	0.0972	3.0700	Class 1
pAmpk	Signaling protein	0.1306	58.6959	Class 2
pAkt (S473)	Signaling protein	3.4715	2.6472	Class 3
pAkt (T308)	Signaling protein	4.5216	2.6716	Class 3
pErk	Signaling protein	1.1824	2.5000	Class 3
pIrs1 (Y612)	Signaling protein	1.5696	4.0356	Class 3
pIrs1 (Y632)	Signaling protein	0.7986	2.6141	Class 3
pJnk	Signaling protein	8.8729	19.6254	Class 3
pAtf2	Transcription factor	0.2231	5.4705	Class 1
pCreb	Transcription factor	0.2283	2.7301	Class 1
pFoxo1	Transcription factor	0.4154	7.9761	Class 1
pJun	Transcription factor	3.6857	26.7482	Class 3
Jun	Transcription factor	4.0469	60.1416	Class 4
Egr1	Transcription factor	4.6078	45.7199	Class 4
Hes1	Transcription factor	6.6499	74.7393	Class 4
peIF4ebp1	Protein-synthesis related factor	0.0791	15.6366	Class 1
peIF4b	Protein-synthesis related factor	0.4978	11.3228	Class 1
pS6	Protein-synthesis related factor	0.1263	19.5381	Class 1

Table S6. Time series of metabolome data in response to insulin stimulation, Related to Figure 4.

Table S7. Classification of insulin-responsive metabolites (IRMs), Related to Figure 4.

Table S8. Identification of allosteric regulators, Related to Figure 4.

Table S9. Identification of responsible metabolic enzymes, Related to Figure 4.

Table S10. Primer sequences used for qRT-PCR measurements, Related to Figure 6.

Gene name	Forward	Reverse
B3galt1	AATGGCGGGCCAATCAG	CAGGGTACAAATCCCTAGGCATA
Creb3l2	TGGTCGTTGTGCTTTGCTTT	GATACAGCCCGTAGCCTTGAAA
Creb3l3	TGGATCCGCTAACGTTGCA	GCCCCTCGCCTTGCTT
Egr1	GACCACAGAGTCCTTTTCTGA	TCACAAGGCCACTGACTAGG
Ehhadh	TCCGGGCAGGCTAAAGC	TGACCACTTATTTGCAGACTTTTCA
G6pase	CAGCCCGTGTAATGAGTAGC	GATGAGTCCTATGGCACGCAGACCT
Hes1	CAACACGACACCGGACAAAC	CGGAGGTGCTTCACTGTCAT
Hmgcr	CTGGGCCCCACGTTCA	ATGGTGCCAACTCCAATCACA
Jun	TGGGCACATCACCACTACAC	GGGCAGCGTATTCTGGCTAT
Lpin1	CCGTGTCATATCAGCAATTTGC	GACCACGAGGTTGGGATCAT
Mat2a	CTTGGTTACGCCCAGATTCTAAA	CACAGCACCTCGATCTTGCA
Msmo1	TCACGATTTCCACCACATGAA	TGTCCCACCACGTGAAGGT
Pck1	CGCTATGCGGCCCTTCT	AGCCAGTGCGCCAGGTACT
Srf	CACGACCTTCAGCAAGAGGAA	CAGCGTGGACAGCTCATAAGC
Upp2	TGGTGGGAGCTCGAACAGA	AACCCGAGTTCCTTGTGCAT

Table S11. Details of resources, Related to Figure 6.

REAGENT or RESOURCE	SOURCE	IDENTIFIER
Antibodies		
Anti-Phospho-Irs Tyr612	Abcam	Cat#ab66153; RRID:AB_1140753
Anti-Phospho-Irs Tyr632	Santa Cruz	Cat#SC17196; RRID:AB_669445
Anti-phospho-Akt Ser473	Cell signaling technology	Cat#4060; RRID:AB_2315049
Anti-Phospho-Akt Thr308	Cell signaling technology	Cat#9275; RRID:AB_329828
Anti-Phospho-S6k Thr389	Cell signaling technology	Cat#9205; RRID:AB_330944
Anti-Phospho-Gsk3β Ser9	Cell signaling technology	Cat#9336; RRID:AB_331405
Anti-Phospho-Erk1/2 Thr202/Tyr204	Cell signaling technology	Cat#9101; RRID:AB_331646
Anti-Phospho-p38 Thr180/Tyr182	Cell signaling technology	Cat#9211; RRID:AB_331641
Anti-Phospho-Sapk/Jnk Thr183/Tyr185	Cell signaling technology	Cat#4668; RRID:AB_2307320
Anti-Phospho-Ampkα Thr172	Cell signaling technology	Cat#2531; RRID:AB_330330
Anti-Phospho-Tsc2 Thr1462	Cell signaling technology	Cat#3617; RRID:AB_490956
Anti-Phospho-Foxo1 Ser256	Cell signaling technology	Cat#9461; RRID:AB_329831
Anti-Phospho-Creb Ser133	Cell signaling technology	Cat#9191; RRID:AB_331606
Anti-Phospho-Atf2 Thr71	Cell signaling technology	Cat#9221; RRID:AB_2561045
Anti-Phospho-c-Jun Ser73	Cell signaling technology	Cat#3270; RRID:AB_2129572

Anti-Egr1	Cell signaling technology	Cat#4154; RRID:AB_2097035
Anti-c-Jun	Cell signaling technology	Cat#9165; RRID:AB_2130165
Anti-HES1	Cell signaling technology	Cat#11988
Anti-Phospho-S6 Ser235/236	Cell signaling technology	Cat#2211; RRID:AB_331679
Anti-Phospho-4elf4ebp1 Ser65	Cell signaling technology	Cat#9451; RRID:AB_330947
Anti-Phospho-eIf4b Ser422	Cell signaling technology	Cat#3591; RRID:AB_10080112
Anti-Rabbit IgG, Peroxidase-conjugated	GE Healthcare	Cat#NA9340V; RRID:AB_772206
Anti-Mouse IgG, Peroxidase-conjugated	GE Healthcare	Cat#NXA931; RRID:AB_772209
Anti-Goat IgG, Peroxidase-conjugated	Sigma-Aldrich	Cat#A-5420; RRID:AB_258242
Anti-Puromycin	Kerafast	Cat#EQ0001 RRID:AB_2620162
Chemicals, Peptides, and Recombinant Proteins		
Human Insulin	SIGMA	Cat#12643-50MG
Deposited Data		
Raw phosphoproteome data	Yugi et al, 2014	S0000000476
Raw RNA-seq data	Sano et al., 2016	DRA: DRA004341
Experimental Models: Cell Lines		
Rat hepatoma cell lines	Laboratory of Shinya Kuroda	RRID:CVCL_0269

Software and Algorithms		
Kyoto Encyclopedia of Genes and Genomes (KEGG)	Kanehisa et al., 2017	http://www.kegg.jp/; RRID:SCR_012773
NetPhorest	Miller et al., 2008; Horn et al., 2014	http://netphorest.info/
bioDBnet	Mudunuri et al., 2009	https://biodbnet-abcc.ncifcrf.gov/
VANTED	Junker et al., 2006	https://immersive-analytics.infotech.monash.edu/vanted/; RRID:SCR_001138
enoLOGOS	Workman et al., 2005	http://biodev.hgen.pitt.edu/cgi-bin/enologos/enologos.cgi
iceLogo	Colaert et al., 2009	http://iomics.ugent.be/icelogoserver/index.html
TRANSFAC Pro	Matys et al., 2006	http://www.gene-regulation.com/pub/databases.html#transfac; RRID:SCR_005620
Match	Kel et al,. 2003	http://gene-regulation.com/pub/programs.html
BRENDA	Schomburg et al., 2013	http://www.brenda-enzymes.org; RRID:SCR_002997

Transparent Methods

Step I: Connection of the IRGs and the TFs

FAO Rat Hepatoma Cells

Rat FAO hepatoma cells (RRID:CVCL_0269, male) were seeded at a density of 3×10^6 cells per dish on 6-cm dishes (Corning) or 1.3×10^6 cells per well on six-well plates (Iwaki) and cultured in RPMI 1640 supplemented with 10% (v/v) fetal bovine serum at 37ºC under 5% CO_2 for 2 days before deprivation of serum (starvation). The cells were washed twice with phosphate-buffered saline (PBS) and starved for 16 hours in serum-free medium including 0.01 nM insulin (Sigma-Aldrich) and 10 nM dexamethasone (Wako), which increases the expression of gluconeogenesis genes, such as *G6pase* and *Pck1* (Lange et al., 1994). We continuously added 0.01 nM insulin before the stimulation, and 0.01 nM insulin was present throughout the experiments unless otherwise specified to mimic *in vivo* basal secretion during fasting (Polonsky et al., 1988). The medium was changed at 4 and 2 hours before the stimulation. Cells were stimulated with the indicated doses of insulin.

Identification of the IRGs

In this study, we used published datasets of the RNA-sequence (RNA-seq) (DDBJ: DRA004341) (Sano et al., 2016) of a time series of insulin stimulation of FAO cells (RRID:CVCL_0269, male). FAO cells were stimulated with 0.01, 1, and 100 nM insulin for 0, 15, 30, 60, 90, 120, and 240 min. In our previous study (Sano et al., 2016), the fragments per kilobase of transcript per million mapped reads (FPKM) values were calculated using Cufflinks (Trapnell et al., 2009, 2012), and 490 differentially expressed transcripts were identified using Cuffdiff (Trapnell et al., 2009, 2012). Among the genes corresponding to these 490 differentially expressed transcripts, the 433 genes, of which FPKM values were calculated at all time points, were defined as IRGs.

Definition of upregulated and downregulated IRGs

The fold changes of FPKMs against those at 0 min were calculated for each IRG. The fold changes were logarithmically transformed to make the range of upregulation and downregulation comparable, and the logarithms were normalized between 0 and 1 to exclude the influence of constitutive expression. We defined the *Pt* value as an index of expression

variation by taking the sum of the absolute values of the differences in the slopes at specific time points and at earlier or later time points, in response to 0.01 nM and 100 nM insulin stimulation (Figure S1B). A smaller *Pt* value indicates that the time series of gene expression has less variability. We defined *AUC_ratio* as an index of response by taking the ratio of *AUC* in response to 100 nM and that in response to 0.01 nM insulin (Figure 1C). The larger the absolute value of the *AUC_ratio* indicates that the response to insulin is larger. Here, genes with a *Pt* value larger than 0.2 were excluded from IRGs because of low quality of quantification. Among the IRGs with *Pt* values that were less than 0.2, those with an *AUC_ratio* of more than $2^{0.5}$ were defined as upregulated IRGs, and those with an *AUC_ratio* of less than $2^{-0.5}$ were defined as downregulated IRGs (Table S1).

Calculation of the EC_{50} and the $T_{1/2}$ values

EC_{50} was defined as the dose of insulin that gives the 50% of the maximal *AUC* of time series of responses (Figure 1C). A smaller EC_{50} indicates a higher sensitivity to insulin dose. To exclude the influence of variability in response over time, we used the *AUC* of the time courses in response to each dose of insulin to calculate EC_{50}. $T_{1/2}$ was defined as the time when the response reached 50% of the peak amplitude (Figure 1C). A smaller $T_{1/2}$ indicates a faster response. The $T_{1/2}$ values for the IRGs, the IRMs, and proteins were calculated from the time course in response to 100 nM insulin stimulation. The distributions of the EC_{50} and $T_{1/2}$ values for IRGs under various thresholds of Cuffdiff (*FDR* < 0.01, 0.03, 0.05, 0.07, and 0.10; default: *FDR* < 0.05) were compared to confirm that the distributions of the EC_{50} and the $T_{1/2}$ were stable.

Wilcoxon rank sum test

Statistical comparisons of the medians of the EC_{50} and $T_{1/2}$ values between the upregulated and downregulated IRGs or between the increased and decreased IRMs were performed using Wilcoxon rank sum test (Gibbons and Chakraborti, 2011; Hollander et al., 2015). The *p* values were adjusted for multiple testing with the Benjamini-Hochberg correction (Bonferroni, 1936) using MATLAB function *mafdr*.

Classification of the IRGs

To characterize the upregulated and the downregulated IRGs by sensitivities and time constants against insulin stimulation, we used EC_{50} and the $T_{1/2}$ values. For the distributions of the EC_{50} and the $T_{1/2}$ values estimated based on the transcriptomic data, we determined the thresholds dividing high or low sensitivity and fast or slow responses using Otsu's method (Otsu, 1979). Using the thresholds, we classified the upregulated or the downregulated IRGs into four classes: Class 1, high sensitivity (EC_{50} < threshold) and fast response ($T_{1/2}$ < threshold) and; Class 2, high sensitivity and slow response ($T_{1/2}$ > threshold); Class 3, low sensitivity (EC_{50} > threshold) and fast response, and Class 4, low sensitivity and slow response.

Functional Enrichment Analysis

The functions of the IRG sets classified by the time constants (fast and slow responsive) or the sensitivity (high and low sensitive) were statistically determined using the DAVID tool (https://david.ncifcrf.gov/home.jsp) (Huang et al., 2009b, 2009a), by examining Gene ontology (GO) of biological process (GOTERM_BP_DIRECT), cellular component (GOTERM_CC_DIRECT), and molecular function (GOTERM_MF_DIRECT), and KEGG pathways (KEGG_PATHWAY). Whole rat genome was used as the background (default). The *p* values were adjusted for multiple testing with the Benjamini-Hochberg correction (Bonferroni, 1936) using MATLAB function mafdr.

Inference of TFs regulating each IRGs

We predicted the TFs that regulate the expression of the classified IRGs by TF binding motif prediction and motif enrichment analysis. The flanking regions around the major transcription start site of each IRG were extracted from Rnor_5.0 (Ensembl, release 73) using Ensembl BioMart (Kinsella et al., 2011). We considered the genomic regions from -300 bp to +100 bp of the consensus transcription start sites as the flanking regions, according to the FANTOM5 time course analysis (Arner et al., 2015). We predicted the TF binding motifs that can bind to each flanking region using a TF database, TRANSFAC Pro (Matys et al., 2006), and Match, a TF binding motifs prediction tool. We used extended *vertebrate_non_redundant_min_SUM.prf*, one of the parameter sets prepared in TRANSFAC Pro for the threshold of similarity score calculated by Match. Because some of the TFs known to be regulated by insulin, including Foxo1, are not included in this parameter set, we

extracted from *vertebrate_non_redundant.prf* the TF binding motifs that were not included in *vertebrate_non_redundant_min_SUM.prf* but were present in TFs included in KEGG *insulin signaling pathway* (rno4910), and we appended these TF binding motifs and their parameters to *vertebrate_non_redundant_min_SUM.prf*. The binding sites within each flanking region were predicted using Match with the extended *vertebrate_non_redundant_min_SUM.prf*.

Motif Enrichment Analysis

The upregulated and the downregulated IRGs were classified into four classes according to individually estimated EC_{50} and $T_{1/2}$ values, and enrichment of binding sites of TF binding motifs in each class was determined using motif enrichment analysis. The enrichment of TF binding motif binding sites in the flanking regions of IRGs in each class were determined by Fisher's exact test (Fisher, 1922) with FDR using Storey's procedure (Storey et al., 2004). The TFs related to significantly enriched TF binding motifs ($FDR < 0.1$) were identified as the TFs regulating IRGs in each class.

Confirmation of the TF predictions using data from the ChIP-Seq Atlas

The genomic regions from ±1000 bp of the consensus transcription start sites as the flanking regions of genes interest bind with the TFs at one or more datasets were defined as target genes for each TF. ChIP-Atlas includes the major TFs in insulin signaling such as Foxo1, Creb1, Egr1, and Hes1. Note that some TFs, such as Foxo1, are not included in the datasets in the liver or hepatocytes.

Step II: Connection of the TFs and the signaling layer

Identification of the IRpPs

In this study, we used published datasets of the quantitative phosphoproteome (JPOST: S0000000476) (Yugi et al., 2014) of a time series of insulin stimulation of FAO cells. FAO cells were stimulated with 1 nM insulin for 0, 2, 5, 10, 30, 45, and 60 min. Cell lysate digested with LysC and trypsin were subjected to Fe-IMAC and iTRAQ labeling for the enrichment of phosphopeptides and quantification by mass spectrometry. All samples were analyzed with a QSTAR Elite (AB Sciex) instrument equipped with a Paradigm MS4 HPLC pump and HTC-PAL autosampler (CTC Analytics AG). The peak lists were generated using Analyst

Mascot.dll v1.6b27 (AB SCIEX). A MASCOT search was performed with the following parameter settings: Trypsin as the enzyme used; the allowed number of missed cleavages as 2; iTRAQ label at the NH_2-terminus, Lys, and carbamidomethylation of Cys as fixed modifications; oxidized Met, iTRAQ label on Tyr, pyroglutamination of NH_2-terminal Glu or Gln, and phosphorylation on Ser, Thr, and Tyr as variable modifications; precursor mass tolerance as 100 ppm; and tolerance of MS/MS ions as 0.2 Da. Assigned rank 1 peptide sequences (MASCOT score >20) were extracted. Evaluation of phosphorylation sites were performed at a post-MASCOT search with in-house script. Because the phosphoproteome data consists of two different time series from two separate experiments (0, 5, 10, and 45 min and 2, 10, 30, and 60 min), some of the phosphopeptides were identified and quantified in data from only one of the time series. Therefore, we calculated a fold change of phosphorylation intensity as a ratio of the phosphorylation intensity at each time point to the phosphorylation intensity at t = 0 or 2 min. A phosphopeptide with a phosphorylation intensity greater than a 1.5-fold increase or less than a 0.67-fold decrease at more than one time point was defined as a quantitatively changed phosphopeptide. We obtained 3,288 phosphopeptides that changed in response to insulin stimulation and defined the proteins including the phosphopeptides as insulin-responsive phosphoproteins (IRpPs).

Over-representation analysis of the IRpPs

We performed over-representation analysis of the IRpPs in signaling pathways, which were the pathways in KEGG database including the character string of “signaling pathway” in their names. To define the signaling layer, we integrated the 15 signaling pathways in which the IRpPs were significantly over-represented, and then removed the proteins for which transcripts were not expressed in FAO cells (Sano et al., 2016) and those that are not located in downstream of InsR (Figure 3A). The identifiers of the IRpPs provided as IPI (Kersey et al., 2004) were converted to KEGG gene identifiers using bioDBnet (Mudunuri et al., 2009). Over-representation of the IRpPs in each signaling pathway was determined by Fisher’s exact test (Fisher, 1922) with FDR using Storey’s procedure (Storey et al., 2004). The signaling layer was constructed by integrating the significantly over-represented signaling pathways ($FDR < 0.1$).

Identification of signaling proteins regulating the TFs

Using the accession numbers from TRANSFAC, we associated the significantly enriched TF binding motifs with TFs using the correspondence obtained from *matrix.dat* in TRANSFAC Pro. The accession numbers of TFs provided in TRANSFAC Pro are associated with the gene IDs for DATF, EMBL, FLYBASE, MIRBASE, PATHODB, PDB, SMARTDB, SWISSPROT, TRANSCOMPEL, or TRANSPATH. To identify regulators of the TFs, the gene IDs of EMBL, PDB, or SWISSPROT that were associated with the accession numbers of human, mouse, and rat TF were converted to KEGG gene IDs using bioDBnet (https://biodbnet-abcc.ncifcrf.gov/) (Mudunuri et al., 2009). We manually determined the upstream molecules of the TFs from the pathway information of KEGG, and except for those in the diseases related pathways (rno05XXX), these were defined as regulators. The regulators included in the signaling layer were extracted and connected to the predicted TFs.

Western blotting of signaling proteins and TFs

We measured the abundance or phosphorylation status of the predicted TFs and the signaling proteins in the signaling layer using Western blotting. The FAO cells were washed with ice-cold PBS and proteins were extracted with 50 mM Tris-Cl pH 8.8 + 1% SDS at the indicated times after insulin stimulation. The lysates were sonicated and centrifuged at 12,000 × *g* at 4 ºC for 15 min to remove debris. Total protein concentration of the resulting supernatants was determined with the bicinchoninic acid assay (Thermo Fisher Scientific) and adjusted to 0.75 mg/mL. Equal amounts of total protein were loaded for SDS-PAGE followed by Western blotting with the antibodies recognizing the indicated proteins or phosphoproteins. Band intensities were measured by using TotalLab Quant software (Nonlinear Inc.). Lysate mixture of FAO cells stimulated with or without 100 nM insulin for 5 min was used as an internal standard to normalize the band intensities for each membrane.

Classification of the signaling proteins and the TFs

To characterize the signaling molecules and the TFs by sensitivities and time constants for insulin stimulation, we classified these using the EC_{50} and the $T_{1/2}$ values, as with the upregulated and the downregulated IRGs. For the distributions of the EC_{50} and the $T_{1/2}$ values from Western blotting data, we determined the thresholds dividing high or low sensitivity and fast or slow responses using Otsu's method (Otsu, 1979). Using the thresholds, we classified the signaling molecules and the TFs into four classes: Class 1, high sensitivity

(EC_{50} < threshold) and fast response ($T_{1/2}$ < threshold) and; Class 2, high sensitivity and slow response ($T_{1/2}$ > threshold); Class 3, low sensitivity (EC_{50} > threshold) and fast response, and Class 4, low sensitivity and slow response.

Measurement of protein synthesis

Protein synthesis was measured as described (Aviner et al., 2014). Briefly, cells were stimulated with the indicated doses of insulin for 3 hours, and 1 μM puromycin was added for the last 2 hours. Cells were washed with ice-cold PBS and proteins were extracted with 50 mM Tris-Cl pH 8.8 including 1% SDS at 3 hours after insulin stimulation. The lysates were sonicated and centrifuged at 12,000 × *g* at 4 ºC for 15 min to remove debris. Total protein concentration of the resulting supernatants was determined with the bicinchoninic acid assay (Thermo Fisher Scientific) and adjusted to 0.75 mg/mL. Equal amounts of total protein were loaded for SDS-PAGE followed by Western blotting with the antibodies to puromycin. All band intensities were measured by using TotalLab Quant software (Nonlinear Inc.) and summed. The values were normalized with cells stimulated with that at 0.01 nM insulin.

Step III: Connection of the IRMs and the IRGs of metabolic enzymes

Metabolomic analysis

The FAO cells were washed at the indicated times after insulin stimulation with 4 mL ice-cold 5% mannitol twice and metabolites were extracted with 1 mL of ice-cold methanol that included the reference compounds [25 μM L-methionine sulfone (Wako), 25 μM 2-Morpholinoethanesulfonic acid, monohydrate (Dojindo), and 25 μM D-Camphor-10-sulfonic acid (Wako)] for normalization of peak intensities of mass spectrometry among samples. The resulting supernatant (400 μL) was sequentially mixed with 200 μL of water and 400 μL of chloroform and then centrifuged at 12,000 × *g* for 15 min at 4ºC. The separated aqueous layer was filtered through a 5 kDa cutoff filter (Millipore) to remove proteins. The filtrate (320 μL) was lyophilized and dissolved in 50 μL water including reference compounds [200 μM each of trimesate (Wako) and 3-aminopyrrolidine (Sigma-Aldrich)] for migration time and then injected into the capillary electrophoresis time-of-flight mass spectrometry (CE-TOFMS) system (Agilent Technologies) (Ishii et al., 2007; Soga et al., 2006, 2009).

Identification of the IRMs

We obtained metabolomic data with nine doses of insulin over a time course of 240 min. We identified IRMs based on the metabolomic data by comparing three factors: temporal changes of metabolites against the value at 0 min, changes in response to 0.01 and 100 nM insulin stimulation at each time point, and the data acquired on different days (n=3). Response of each metabolite to insulin doses was determined by three-way analysis of variance (ANOVA) comparing three factors: temporal changes of metabolites against the value at 0 min, responses to 0.01 and 100 nM insulin stimulation at each time points, and the data acquired on different days (n=3). The fold change of abundance of metabolites relative to the mean abundance at 0 min was calculated for each metabolite. We calculated log_2 values of the fold changes so that ranges of increased and decreased IRMs become comparable. We performed three-way ANOVA with insulin doses (0.01 and 100 nM), time points after insulin stimulation (0, 5, 15, 30, 60, 90, 120, and 240 min), and data sets using the logarithmic values of fold changes. The p values against insulin doses were calculated and the FDR for each metabolite was calculated by Storey's procedures (Storey et al., 2004). The λ value to calculate FDR was set to 0.8 with reference to the distribution of p values. The metabolites showing significance ($FDR < 0.1$) were defined as IRMs.

Definition of the increased and the decreased IRMs

Increased and decreased IRMs were defined using the same procedure that we used to identify the upregulated and downregulated IRGs. For each IRM, the fold change in the abundance of metabolites at each time point relative to the mean abundance at 0 min was calculated. We calculated log_2 values of the fold changes so that the ranges of increased and decreased IRMs were comparable. The logarithmic values of fold change were normalized between 0 and 1, and the AUC_ratio was determined as the ratio of AUC with 100 nM insulin to AUC with 0.01 nM stimulation. The metabolites with an AUC_ratio of more than $2^{0.5}$ were defined as increased IRMs, and those with the AUC_ratio of less than $2^{-0.5}$ were defined as decreased IRMs.

Classification of the increased and the decreased IRMs

To characterize the increased and the decreased IRMs by sensitivities and time constants against insulin stimulation, we used the EC_{50} and the $T_{1/2}$ values, as with the upregulated and the downregulated IRGs. For the distributions of the EC_{50} and the $T_{1/2}$ values calculated from

the metabolomic data, we determined the thresholds dividing high or low sensitivity and fast or slow responses using Otsu's method (Otsu, 1979). Using the thresholds, we classified the increased or the decreased IRMs into four classes: Class 1, high sensitivity (EC_{50} < threshold) and fast response ($T_{1/2}$ < threshold) and; Class 2, high sensitivity and slow response ($T_{1/2}$ > threshold); Class 3, low sensitivity (EC_{50} > threshold) and fast response, and Class 4, low sensitivity and slow response.

Identification of allosteric regulation

Many metabolic enzymes are regulated allosterically by metabolites; therefore, we identified IRMs that function as allosteric regulators for metabolic enzymes using the BRENDA database, which is a database with information regarding allosteric effectors and their target enzymes (Schomburg et al., 2013). A metabolite can operate as an activator for some enzymes and as an inhibitor for others. We identified allosteric regulation for metabolic enzymes using procedures from Yugi et al., 2014. We obtained the entries for metabolic enzymes from the BRENDA database (http://www.brenda-enzymes.org) (Schomburg et al., 2013) and extracted their allosteric effector (activator and inhibitor) information, as reported for mammals (*Bos Taurus, Felis catus, Homo sapiens*, "Macaca", "Mammalia", "Monkey", *Mus booduga, Mus musculus, Rattus norvegicus, Rattus rattus, Rattus* sp., *Sus scrofa*, "dolphin", and "hamster"). Then, we associated the standard compound names of allosteric effectors used in BRENDA with metabolite names that were used in KEGG to obtain the KEGG compound ID related to each allosteric effector. We defined as "activating event", if the amount increases for an allosteric effector that positively regulates the enzymatic activity or if the amount decreases for an allosteric effector that negatively regulates the enzymatic activity. We defined as "inhibitory event", if the amount decreases for an allosteric effector that positively regulates the enzymatic activity or if the amount increases for an allosteric effector that negatively regulates the enzymatic activity. These "activating events" and "inhibitory events" were classified into four classes according to the sensitivity and time constant of the IRMs that are allosteric effectors and projected onto KEGG *metabolic pathway* (Figure S4C, Table S8).

Step IV: Construction of the trans-omic network by insulin stimulation

Identification of IRGs encoding metabolic enzymes

The genes in the transcriptome data were annotated based on Rnor_5.0 (Ensembl, release 73), and the Ensembl gene identifiers of the IRGs were converted to KEGG gene identifiers using bioDBnet (https://biodbnet-abcc.ncifcrf.gov/) (Mudunuri et al., 2009). The genes encoding metabolic enzymes were defined as those included in *metabolic pathways* (rno01100), a global metabolic pathway of KEGG database. We determined 23 of the upregulated or downregulated IRGs encoded metabolic enzymes.

Step V: *in vivo* validation of selective trans-omic networks by induced and basal insulin stimulation

Sprague-Dawley rats (insulin-clamp)

All rat studies were approved by the Kyushu University Institutional Animal Care and Use Committee. The Sprague-Dawley (SD) rats (RRID:RGD_1566457) (male, 10 week old) were purchased from Japan SLC Inc. After overnight fasting, we anesthetized rats with isoflurane. To suppress endogenous insulin secretion, we administered somatostatin through the jugular vein (3 μg/kg per min). Insulin was administered through the mesenteric vein at the indicated dose, maintaining the blood glucose concentration at a constant amount (150 mg/dl). Blood was sampled at the indicated time points, and blood insulin amounts were measured using a rat insulin enzyme-linked immunosorbent assay kit (Shibayagi Co. Ltd.). At the indicated time points, the rats were killed, and the livers were immediately frozen with liquid nitrogen (Matveyenko et al., 2012).

Western blotting for the insulin-clamped rat livers

The insulin-clamped rats were killed at the indicated time points, and the livers were immediately frozen with liquid nitrogen (Matveyenko et al., 2012). The livers were washed with ice-cold PBS and proteins were extracted with 50 mM Tris-Cl pH 8.8 + 1% SDS at the indicated times after insulin injection. The lysates were sonicated and centrifuged at 12,000 × *g* at 4 ºC for 15 min to remove debris. Total protein concentration of the resulting supernatants was determined with the bicinchoninic acid assay (Thermo Fisher Scientific) and adjusted to 0.75 mg/mL. Equal amounts of total protein were loaded for SDS-PAGE

followed by Western blotting with the indicated antibodies. Band intensities were quantified by using TotalLab Quant software (Nonlinear Inc.). The Western blotting measurements were performed three times independently. Details of the antibodies are described in Table S11.

Quantitative reverse transcription polymerase chain reaction (qRT-PCR) for the insulin-clamped rats

The insulin-clamped rats were killed at the indicated time points, and the livers were immediately frozen with liquid nitrogen (Matveyenko et al., 2012). The livers were harvested, and total RNA was isolated using RNeasy Mini Kit (Qiagen). Total RNA was reverse-transcribed into cDNA using the QuantiTect Reverse Transcription Kit (Qiagen) according to the manufacturer's protocol. qRT-PCR was performed as previously described (Kubota et al., 2012). Briefly, total RNA was extracted from the rat livers using RNeasy Mini Kit (Qiagen) and reverse-transcribed into complementary DNA (cDNA) using the High-Capacity RNA-to-cDNA Kit (Applied Biosystems) according to the manufacturer's protocol. The cDNA samples were amplified using the Power SYBR Green PCR Master Mix (Applied Biosystems) and the 7300 Real-Time PCR system (Applied Biosystems) according to the manufacturer's protocol. The primer sequences used in the qRT-PCR analysis are listed in Table S10. The qRT-PCR analyses were performed three times independently.

Identification of low- and high-dose insulin responsive molecules and genes

We tested the sensitivity of the rat liver response to insulin dose using data from the low-dose (2 μM) or high-dose (20 μM) insulin-clamped rats obtained by Western blotting and qRT-PCR (Sano et al., 2016; Kubota et al., *accepted*). For Western blotting data, the intensities were normalized for each membrane with the mean of intensity of the samples from animals without insulin injection. For qRT-PCR data, we calculated the relative expression with the *ΔCt* method using the expression of *36B4* as a reference gene and normalized the values using the mean of the relative expression in samples from animals without insulin injection. We confirmed the increase or decrease of the measured molecules and genes using the corrected values. We classified as upregulated IRGs or increased in response to insulin those proteins (Western blot data) or genes (qRT-PCR data) for which the *AUC* values in response to high-dose insulin injection were greater than 1 were used. We classified as downregulated IRGs or decreased in response to insulin those proteins or genes for which the *AUC* values in response to high-dose insulin injection were smaller than 1. The significance of the changes

of the corrected values at each time points after insulin injection against those without insulin injection were tested by Welch's *t*-test using *ttest2* function in MatLab (version R2014a, MathWorks) with one-sided approach. For the Western blotting and qRT-PCR data for the upregulated IRGs, we tested the alternative hypothesis that the population mean of the intensities after insulin injection is greater than that of the intensities without insulin injection. For the qRT-PCR data for the downregulated IRGs, we tested the alternative hypothesis that the population mean of the intensities after insulin injection is smaller than that of the intensities without insulin injection. The FDR values were calculated by Storey's procedure (Storey et al., 2004) using *mafdr* function in MatLab. The proteins and genes significantly changed (FDR < 0.1) at one and more time point in response to both of low- and high-dose insulin injection were defined as low-dose insulin responsive, and those significantly changed in response to only high-dose insulin injection were defined as high-dose insulin responsive. The proteins or genes regarded as "Other" include those not significantly changed at 2 or more time points or significantly changed in response to only low-dose insulin injection. We compared the classification of low- and high-dose insulin responsive *in vivo* to the basal and induced responses we obtained in FAO cells.

Data Availability

The raw phosphoproteome data generated in previous study (Yugi et al., 2014) and used in this study have been deposited in the JPOST under ID code S0000000476. The raw transcriptomic data generated in previous study (Sano et al., 2016) and used in this study have been deposited in the DDBJ under ID code DRA004341. Details are described in Table S11.